Assessment of Plume Rise and Dispersion Models Using Lidar Data

Martin Marietta Corp, Baltimore, MD Environmental Center

Prepared for

Maryland Dept of Natural Resources, Annapolis Power Plant Siting Program

Feb 79

PPSP-MP 24

ASSESSMENT OF PLUME RISE AND DISPERSION MODELS
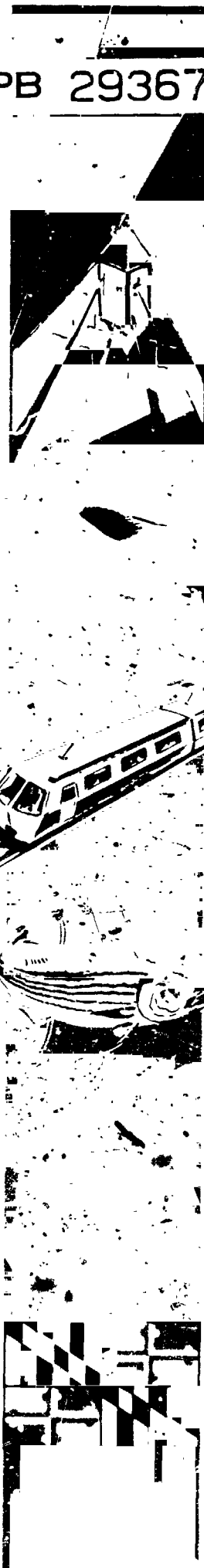
USING LIDAR DATA

Prepared By

Martin Marietta Corporation
Environmental Center
1450 South Rolling Road
Baltimore, Maryland   21227

February 1979

MARYLAND POWER PLANT SITING PROGRAM

BIBLIOGRAPHIC DATA SHEET	1. Report No. PPSP-MP-24	2.	3. Recipient's Accession No. PB293673

4. Title and Subtitle	5. Report Date
Assessment of Plume Rise and Dispersion Models Using Lidar Data	February, 1979
	6.

7. Author(s) Jeffrey C. Weil	8. Performing Organization Rept. No. PPSP-MP-24

9. Performing Organization Name and Address	10. Project/Task/Work Unit No.
Martin Marietta Corporation 1450 South Rolling Road Baltimore, Maryland 21227	11. Contract/Grant No. 1-72-02(79)

12. Sponsoring Organization Name and Address	13. Type of Report & Period Covered
Power Plant Siting Program Tawes State Office Building Annapolis, Maryland 21401	final
	14.

15. Supplementary Notes

16. Abstracts

Predictions from plume rise and dispersion models are compared to field measurements obtained in a recent field experiment sponsored jointly by PPSP and NASA. Lidar measurements of aerosol density, ground level measurements of SO_2, and vertically integrated SO_2 concentrations were gathered.

17. Key Words and Document Analysis. 17a. Descriptors

Lidar, plume rise, plume dispersion, Gaussian plume, air quality

17b. Identifiers/Open-Ended Terms

17c. COSATI Field/Group

18. Availability Statement	19. Security Class (This Report) UNCLASSIFIED	21. No. of Pages 83
release unlimited	20. Security Class (This Page) UNCLASSIFIED	22. Price PC A05/MF A01

ASSESSMENT OF PLUME RISE AND DISPERSION MODELS

USING LIDAR DATA

By

Jeffrey C. Weil
Martin Marietta Corporation
Environmental Center
1450 South Rolling Road
Baltimore, Maryland 21227

February 1979

FOREWORD

This report, comparing mathematical models for plume rise and dispersion to field measurements of plume rise and dispersion at the Morgantown power plant, was prepared for the Maryland Power Plant Siting Program, Department of Natural Resources, by the Environmental Center, Martin Marietta Corporation under Contract Number 1-72-02(79).

The data used in this report were obtained by:

Engineering Test Services
P. O. Box 11
Sandston, Virginia 23150

Environmental Measurements, Incorporated
1445 Old Annapolis Road
Arnold, Maryland 21012

Lidar Applications Branch
National Aeronautics and Space Administration
Langley Research Center
Hampton, Virginia 23665

ACKNOWLEDGEMENTS

CONTENTS

Preceding page blank

Martin Marietta Environmental Center

LIST OF TABLES

LIST OF FIGURES

Martin Marietta Environmental Center

NOMENCLATURE

c	Ground-level SO_2 concentration (ppb)
c_{max}	Maximum predicted ground-level SO_2 concentration (ppb)
c_p	Specific heat of air at constant pressure (kcal/kg/°K)
c_1	Mean of maximum SO_2 concentrations from individual crosswind profiles in a set of repeated profiles on one measurement route (ppb)
c_2	Maximum SO_2 concentration from average crosswind profile (ppb)
F	Buoyancy flux;

$$F = \frac{V_1 g}{\pi} \frac{T_1 - T_1}{T_1} \quad (m^4/sec^3)$$

g	Gravitational acceleration (m/sec²)
h	Height above ground (m)
h_e	Effective stack height (m)
h_s	Physical stack height (m)
H_m	Height of mixing layer (m)
ℓ	Buoyancy length scale; Equation (2) (m)
m_y	Standard deviation of plume centerline crosswind position about its time mean position (m)
q	Sensible upward heat flux, Q_o, times $g/(\rho c_p T)$ (m²/sec³)
Q_o	Sensible upward heat flux from ground (kcal/m²/sec)
r	Local effective plume radius (m)
s_y	Crosswind standard deviation of instantaneous plume (m)
SR	Scattering ratio; backscattered light intensity in presence of plume divided by backscattered light intensity in plume's absence (dimensionless)
t_L	Lagrangian integral time scale (sec)
T	Temperature (°K)
T_1	Stack exit temperature (°K)

Martin Marietta Environmental Center

T_1 — Ambient air temperature at stack height (°K)

u_* — Friction velocity (m/sec)

v — Mean wind speed (m/sec)

V_i — Volume flux at stack exit (m^3/sec)

w_d — Average downdraft velocity in convective mixing layer; Equation (12) (m/sec)

w_* — Convective velocity scale; Equation (14) (m/sec)

x — Distance from stack (m)

x_{max} — Distance from stack to predicted maximum concentration (m)

x^* — Distance from stack where entrainment rate changes; Equations 4 and 7 (m)

X — Downwind distance; Equation (15) (dimensionless)

y — Crosswind distance (m)

z — Plume rise above stack (m)

β — Entrainment parameter in plume rise formula (dimensionless)

β_{yL} — Ratio of mean crosswind standard deviation, $\langle \sigma_y \rangle$, from instantaneous plume profile to local plume rise z (dimensionless)

β_{zE} — Ratio of vertical standard deviation σ_z from average plume profile to local plume rise z (dimensionless)

γ — Exponent of distance in vertical dispersion formula; Equation (21) (dimensionless)

Δh — Final plume rise (m)

ε — Turbulent energy dissipation rate (m^2/sec^3)

η — Distance along line of sight of remote sensing instrument (m)

κ — von Karman constant (=0.4, dimensionless)

ρ — Density (kg/m^3)

σ_y — Crosswind plume standard deviation (m)

$\langle \sigma_y \rangle$ — Average of individual measured crosswind standard deviations from a series of repeated plume profiles (m)

σ_z — Vertical plume standard deviation (m)

$\langle\sigma_z\rangle$ Average of individual measured vertical standard deviations from a series of repeated plume profiles (m)

Subscripts

f   Designates value for distance where final rise occurs

meas   Measured variable

pred   Predicted variable

Martin Marietta Environmental Center

I. INTRODUCTION

Accurate predictions of plume rise and dispersion are necessary to estimate ground-level concentrations of tall stack effluents. Despite much work in developing predictive models for plume rise and spread, there remain a number of problems of practical importance. One is estimating the effect on plume rise when effluents are released from two nearby stacks. If plumes from two nearby stacks combine, they may rise higher than either plume rising individually and may lower the maximum ground-level concentration for the two stacks. A second problem is choosing the appropriate formula, or formulas, (from the many available, see Briggs, 1969) for predicting final rise in neutral or convective atmospheric conditions. Although maximum ground-level concentrations of tall stack effluents in level terrain occur during these atmospheric conditions, there has been a lack of good observations of final rise for these important neutral and convective conditions. A third problem is the lack of generalized formulas for predicting plume spread parameters (e.g., σ_y and σ_z in the Gaussian plume model) in terms of stack exit conditions, meteorological variables, and downwind distance. Generalized formulas and their verification by field data are needed to improve our understanding of plume spread and to improve upon the accuracy of existing empirical formulas for spread.

This report addresses these three problems. Predictions from plume rise and dispersion models are compared to measurements obtained in a recent field experiment sponsored jointly by the Maryland Power Plant Siting Program and the National Aeronautics and Space Administration (NASA). The plume rise study includes a determination of plume rise enhancement, when two nearby stacks were operating, in light of a well-known formula for the initial rise of single

stack plumes and a test of formulas for final rise during neutral and convective conditions. The plume dispersion investigation tests the applicability of free convection scaling (Willis and Deardorff, 1978; Lamb, 1978a, 1978b) to buoyant stack plumes dispersing in convective mixing layers.

The investigations in this report required reliable measurements of the rise and three-dimensional dispersion of buoyant stack plumes. These measurements were obtained with a remote sensing lidar that detects ambient aerosols. The main advantage of a lidar is its ability to make aerosol measurements remotely and at a high resolution in space and time. It has been assumed, as is customarily done (Hamilton, 1967; Johnson and Uthe, 1971), that the plume aerosols were small enough to be dispersed with the stack gases and act as a tracer.

The field work was conducted at the Morgantown power plant during four 1-week periods in September and October 1976, all during nearly neutral or convective atmospheric conditions. In addition to lidar measurements, the field program included measurements of ground-level SO_2 and vertically integrated SO_2 concentrations, both from a mobile van, meteorolog. al conditions, and stack emission characteristics. The lidar data were taken by the Lidar Applications Branch of the NASA Langley Research Center and its subcontractors -- Old Dominion University, Physics and Geophysical Sciences Department, and Wyle Laboratories. The SO_2 concentrations and meteorological conditions were measured by Environmental Measurements, Incorporated, and the stack test data by Engineering Test Services.

In Section II, the experimental program is described, and plume geometry obtained from the lidar data is compared to that from the SO_2 measurements. The plume rise studies are presented in Section III, and the applicability of free convection scaling to buoyant stack plume dispersion is discussed in Section IV.

II. EXPERIMENTAL PROGRAM

A. Power Plant, Instrumentation, and Experimental Procedures

The Morgantown power plant is on relatively flat terrain along the
Potomac River, about 56 kilometers south of Washington, D.C. It has two
575-MWe generating units operating on either coal or oil or a mixture of
the two. Flue gases from each unit are exhausted through a 213-m stack;
the two stacks are 76 m apart. During the September 1976 measurements,
both generating units were in operation, but during the October 1976
measurements, only unit 2 was operating.

For the purposes of the analyses discussed later, only the SO_2
emission rates and the stack buoyancy fluxes were needed. These variables
were computed from the hourly operating logs on fuel consumption, generating
load, and stack temperature, and the weekly analysis of fuel sulfur content.
The range of SO_2 emission rates and buoyancy fluxes is given in Table 1.

Particulate, SO_2, and NO_x emission rates and particle size distribution
were measured during the field program. However, due to sampling and coordi-
nation problems, these measurements were not always made simultaneously with
the lidar and SO_2 measurements. For this reason, the SO_2 emission rates and
buoyancy fluxes were computed from the operating logs for the analyses in
Sections III and IV. For the most part, the SO_2 emissions computed from the
hourly load conditions agreed with the values based on the stack test data.*

---

* The ratio of the SO_2 emission rate calculated from stack tests to that
  calculated from fuel consumption and composition data averaged 1.15, based
  on comparisons for 4 different days.

Table 1. Stack emission characteristics, meteorological conditions, and plume measurements

Stack Height (m)	213
Distance Between Stacks (m)	76
Stack Diameter at Top (m)	6
SO_2 Emission Rate (kg/sec)	
Stack 1	1.69 - 1.75
Stack 2	1.61 - 2.06
Buoyancy Flux (m^4/sec^3)	
Stack 1	704 - 741
Stack 2	704 - 843
Mean Wind Speed (m/sec)	4.3 - 13.7
Mixing Depth (m)	700 - 1650
Solar Insolation ($kcal/m^2/sec$)	0.02 - 0.18
Distance Downwind Covered by Measurements (km)	
Lidar	0.4 - 6.1
Mobile van; SO_2 measurements	2.4 - 25.5
Number of Plume Cross Sections (average profiles, individual profiles)	
Lidar	31, 251
Mobile van	8, 44

The results of the stack tests and a discussion of the sampling procedure were given by Engineering Test Services (1977).

The NASA mobile lidar system consisted of a ruby laser (694 nm radiation), a telescope receiver, a detector package, and associated instrumentation. During field operation, the laser transmitted 1.5 Joule of energy per pulse, with a pulse length of 30 ns and a repetition rate of 1 pulse every 2 seconds. The beam divergence of the laser was 1 mrad. The laser, telescope, and detector were fixed on a searchlight mount equipped with a tracking system to monitor the elevation and azimuth angle. The searchlight mount and associated laser/receiver instrumentation were mounted on a flatbed trailer.

The data collection system consisted of an oscilloscope for a real-time display, and a digitizer, minicomputer, and 9-track tape recorder for data storage. Some data processing was done on a near real-time basis to permit preliminary data analysis and to provide a television monitor display, which permitted a more comprehensive display of the plume than did the oscilloscope. Detailed descriptions of the lidar system are given by Mills et al. (1978) and Browell (1977).

The experimental plan was to locate the lidar at a preselected site 2 km to 4 km from the plant so that the plume could be viewed from the side. A plan view of typical lidar and plume positions is shown in Fig. 1. Aerosol profiles* were measured at several distances downwind of the stacks as shown by the lidar lines-of-sight in Fig. 1. Aerosol profiles at one plume cross

---

* The term "aerosol profiles" here actually means profiles of backscattered light or simply backscatter. To relate the backscatter to the aerosol mass concentration, one must know the size distribution and optical properties of the aerosols. In this study, as is frequently done, we assume that the aerosol size distribution and optical properties are uniform over the plume. The backscatter is then a measure of relative aerosol concentrations within the plume (see Johnson, 1969).
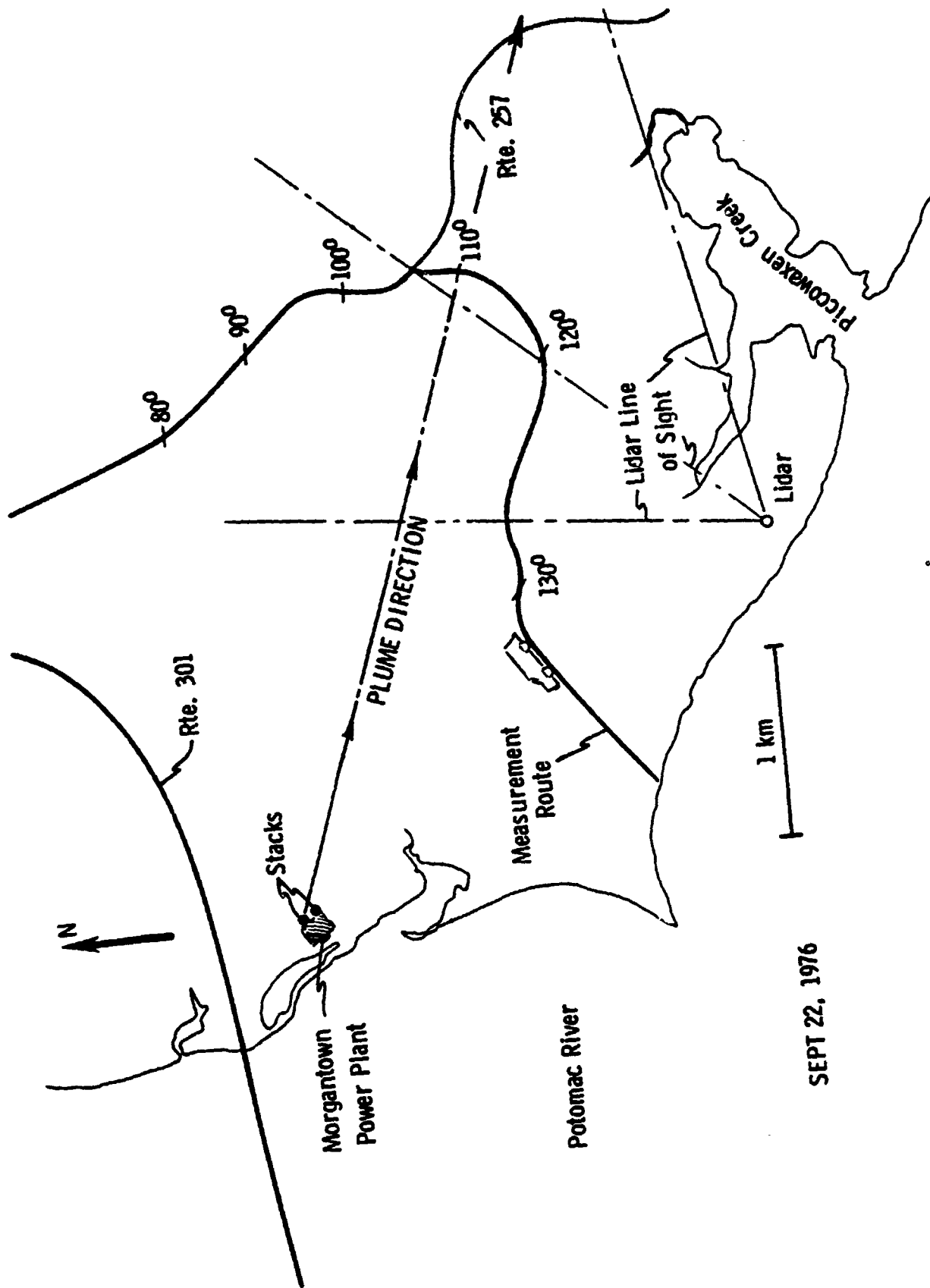
Figure 1. Plan view of typical positions of lidar and plume.

section were obtained by scanning the lidar through elevation angles from near the horizon to an angle sufficiently high that the laser beam was above the plume (as indicated by the real-time display). Profiles were then measured in a like manner at each of the other designated cross sections. The same cross sections were sequentially sampled a number of times so that average aerosol profiles could later be computed for each cross section. Typically, eight scans were taken of three cross sections over about a 1-hour period. Measurements were confined to the first 6 km downwind of the stacks.

Time and the logistics of moving the lidar dictated that a chosen site be used for several days even though it may not have been ideal for each day. Site selection was based on a wind forecast from the National Weather Service. The lidar was located for 1 week at each of the four sites shown in Fig. 2.

The mobile van was equipped with a Barringer correlation spectrometer to measure the vertically integrated SO_2 above the van, and a Meloy total sulfur monitor to measure the ground-level SO_2 concentration. Repeated passes along a road that was nearly transverse to the plume direction were made to obtain crosswind profiles of ground-level and vertically integrated SO_2; typically, six crosswind profiles were measured along the same route during a 1-hour time interval. (See Weil, 1977, and Weil and Jepsen, 1977, for a more detailed description of the measurement procedures.) The SO_2 measurements were made simultaneously with, but not always at the same cross sections as the lidar measurements (due to a lack of roads within about 4 km of the plant). When possible, one of the cross sections scanned by the lidar was selected to coincide (approximately) with one of the mobile van measurement routes. This was done to compare the crosswind plume geometry as determined by the two measurement systems.
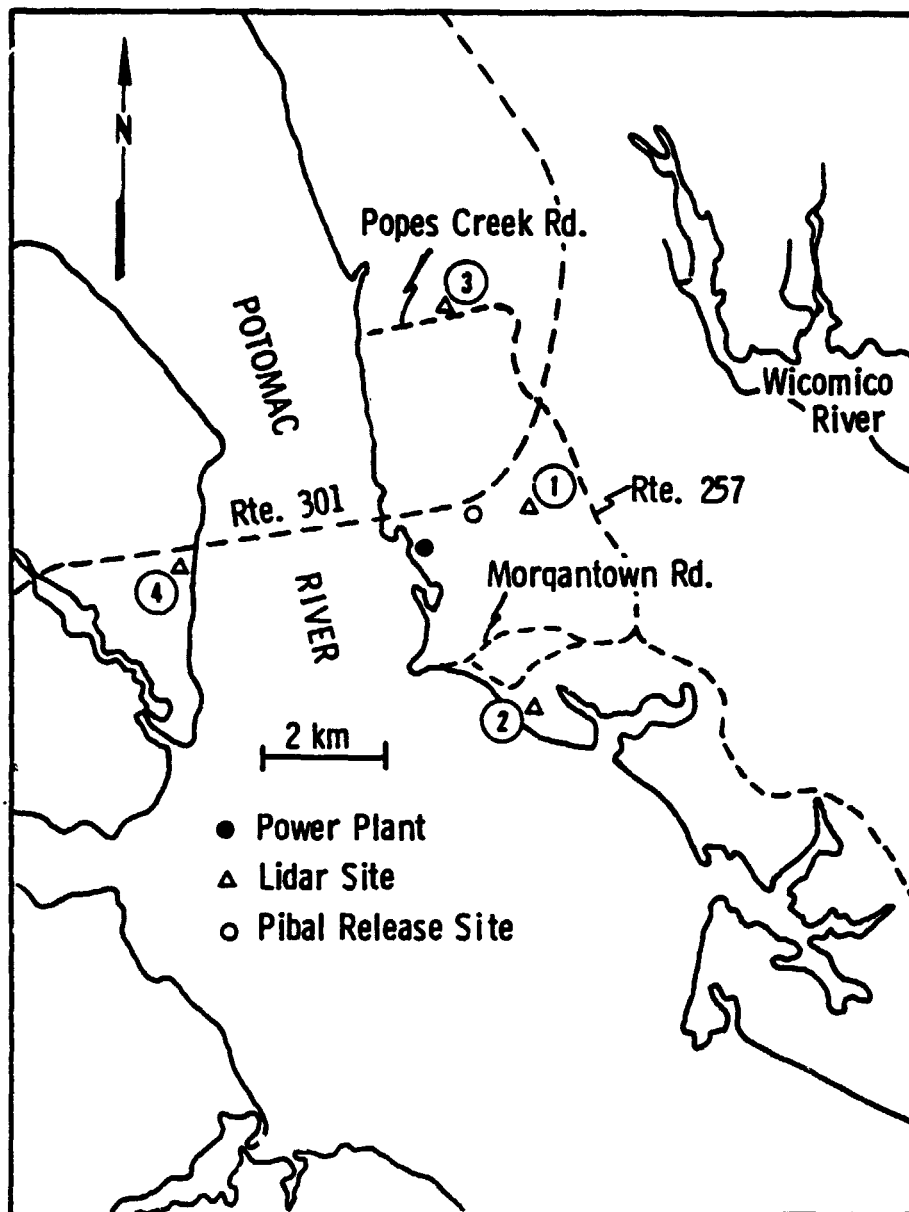
Figure 2. Map of power plant area showing locations of plant, lidar sites, and pilot balloon release site.

Vertical profiles of wind speed and direction were obtained hourly from theodolite tracked pilot balloons (pibals), and vertical temperature profiles were measured three times a day with a balloon-borne temperature sensor. Solar insolation measurements were made on the power plant property with an Eppley pyrheliometer. Surface observations of wind speed, cloud cover, and ceiling height were obtained from the Washington National Airport* for determination of the Pasquill stability class by the Turner (1964) approach.

B. Data Analysis

The height of the convective mixing layer and the temperature gradient within the layer were determined from the observed temperature profiles. Wind speed used in model calculations was an average value within the mixing layer (see Weil, 1977).

The crosswind standard deviation (σ_y) and peak concentration were calculated for each individual ground-level and overhead SO_2 concentration profile. The average standard deviation $\langle\sigma_y\rangle$ and average peak concentration c_1 from individual profiles in a set of repeated passes were used to approximate those of a 10-minute averaged plume.** In addition, an average profile was found by computing the average concentration at 100 equally spaced angular intervals across the composite plume. The σ_y and peak concentration from the average profile were used to approximate those of an hourly averaged plume (see Weil, 1977, and Weil and Jepsen, 1977, for details of the calculations). σ_y's from the vertically integrated SO_2 profiles were used to evaluate

---

* The Washington National Airport is about 56 kilometers north of the Morgantown plant.

** Each individual profile was generally measured in less than 10 minutes.

Martin Marietta Environmental Center

dispersion models in Section IV because they were believed to be more representative of the crosswind distribution of the entire plume than σ_y's from the ground-level SO_2 profiles.

Computation of the plume centroid and standard deviations, σ_y and σ_z, from the lidar data was done by Mills et al. (1978); only a brief description of the procedure is given here. The lidar data were processed to determine the scattering ratio (SR) -- ratio of backscattered light intensity with a plume to backscattered light intensity without a plume -- as a function of crosswind distance and altitude for each observed cross section and for averages of repeated scans of a cross section. Procedures for obtaining the lidar return in the plume's absence are discussed in Mills et al. The distribution of the scattering ratio was used to calculate the location of the plume centroid and the crosswind and vertical plume standard deviations.* Mean values of plume standard deviations from individual cross sections in a set of repeated scans were used to approximate those of a 10-minute averaged plume. Plume standard deviations from the average profile, which includes plume meandering, were used to approximate those of an hourly averaged plume. Plume rise was taken to be the height of the centroid of the average scattering ratio distribution. A list of all data used in this analysis is given in Appendix A.

The crosswind standard deviation was corrected for the angular difference between the lidar line of sight and a normal to the local plume centerline. In Mills et al. (1978), the local plume direction was assumed to be given by the vector from the stack to the centroid (in the crosswind direction) of the lidar profile. This presumes that the plume followed a straight line trajectory. However, a plot of the centroids from cross sections measured simultaneously

---

* Plume standard deviations were computed by taking second moments of the SR distribution about the centroid of the distribution.

but at different downwind distances showed that several plume trajectories were curved. In our analysis, we used the plume direction inferred from the curved trajectory to correct σ_y for the "non-normality" of the lidar line-of-sight. In a few cases, the resultant σ_y was 40 percent greater than the value given by Mills et al.

C. Profiles of Scattering Ratio and SO_2

During the field study, five sets of simultaneous lidar and SO_2 measurements of the same plume cross section were acquired. An example of one of the cross sections is indicated in Fig. 1 (the mobile van measurement route and middle lidar line-of-sight). The average crosswind SO_2 profile extended from an azimuth of 105° on the measurement route to about 120°.

Figure 3 shows a comparison of the hourly average crosswind profiles of vertically integrated scattering ratio and SO_2 concentration obtained from the simultaneous measurements. The concentration and ratio were summed over 200-m crosswind segments and normalized by the respective maximum sum. The shapes of the two profiles are in reasonably good agreement, although the SO_2 profile is somewhat broader than the scattering ratio profile. This may be due to the longer time required to traverse the plume by the mobile van (~ 3 minutes in this case) than to scan it with the lidar (~ 1 minute), and to the lower number of the van passes made (five van passes vs eight lidar scans).

Profiles of SO_2 concentration and scattering ratio obtained during the other four simultaneous measurement periods were generally in good agreement. A discussion of these profiles is given in Appendix B.

Martin Marietta Environmental Center
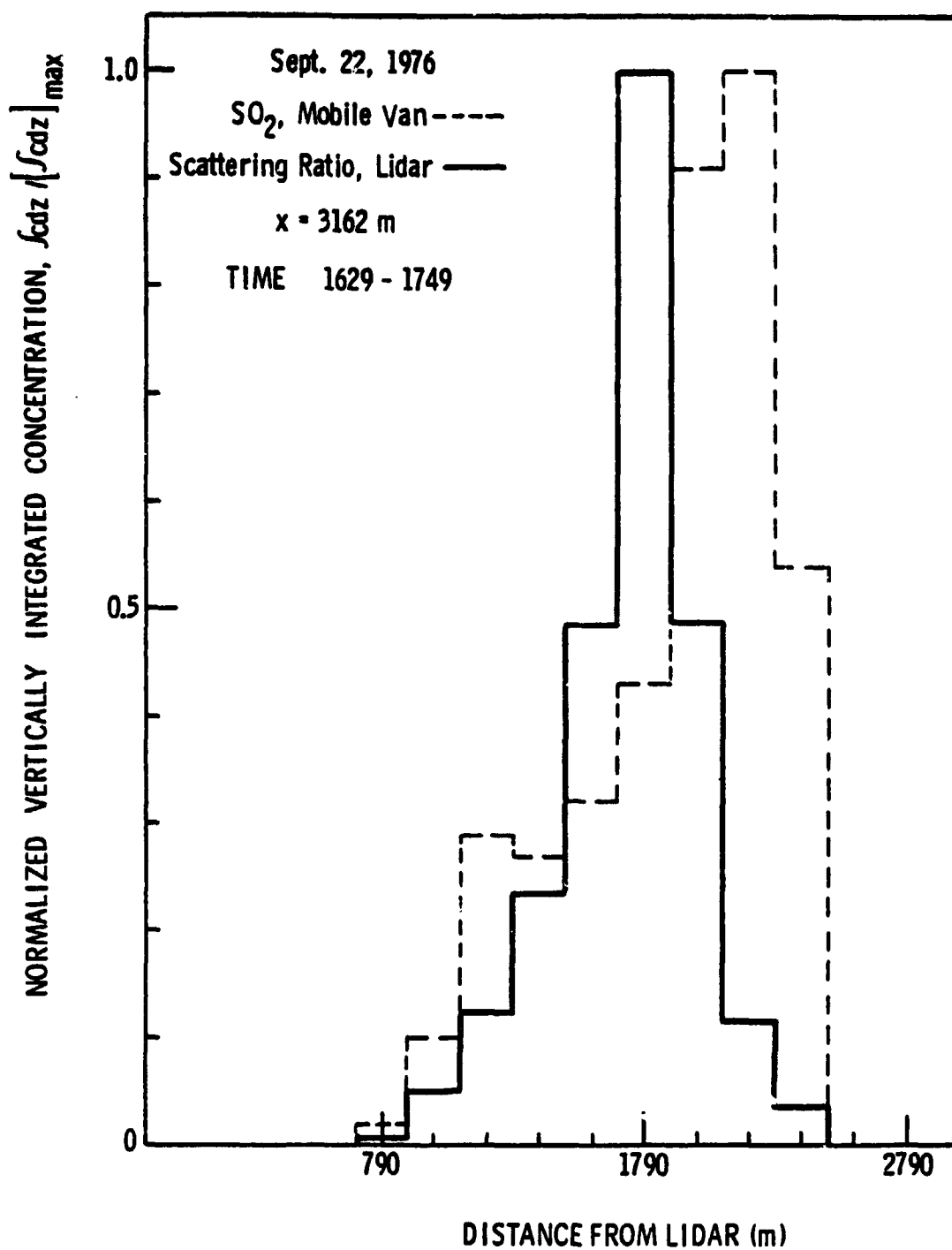
Figure 3. Average crosswind profiles of vertically integrated SO_2 and scattering ratio. (Measurements approximate hourly averaged profiles.)

The lidar data of most interest in this plume modeling study were the vertical distributions of plume material. An example is shown in Fig. 4 where average vertical profiles of the crosswind integrated scattering ratio are plotted for the three lidar cross sections indicated in Fig. 1. The profiles obtained at downwind distances of 2.2 km and 3.2 km from the power plant show that the plume is contained within the mixing layer (determined from an earlier temperature profile*). The elevated concentrations at the top of the middle profile are probably due to the upper stable layer trapping the plume. The profile at 4.9 km indicates that the plume is diffusing into the upper stable layer. The centroid of this last profile is slightly below that measured at the 3.2-km cross section, possibly due to a thermal downdraft.

On one day, simultaneous scans of SO_2, using the Barringer correlation spectrometer, and scattering ratio were obtained from the side of the plume about 1 km downwind of the plant. The spectrometer was fixed on a swiveling tripod mount so that it could scan in azimuth and elevation angles. The spectrometer and lidar were positioned at site 3 (see Fig. 2), and the wind was from the southwest.

A comparison of average profiles of integrated scattering ratio and SO_2 along the lines of sight of the measuring instruments is presented in Fig. 5. The two profiles are in fair agreement. Low concentration tails on the SO_2 profile may be due to an inappropriate choice of the background value of the integrated SO_2. The comparison in Fig. 5, as well as that in Fig. 3, supports the assumption that the aerosols are a good tracer of the SO_2 plume.

---

* A lidar measurement of the ambient aerosol profile at the time of the plume measurements indicated that the mixing depth was about the same as measured by the temperature profile.

Martin Marietta Environmental Center
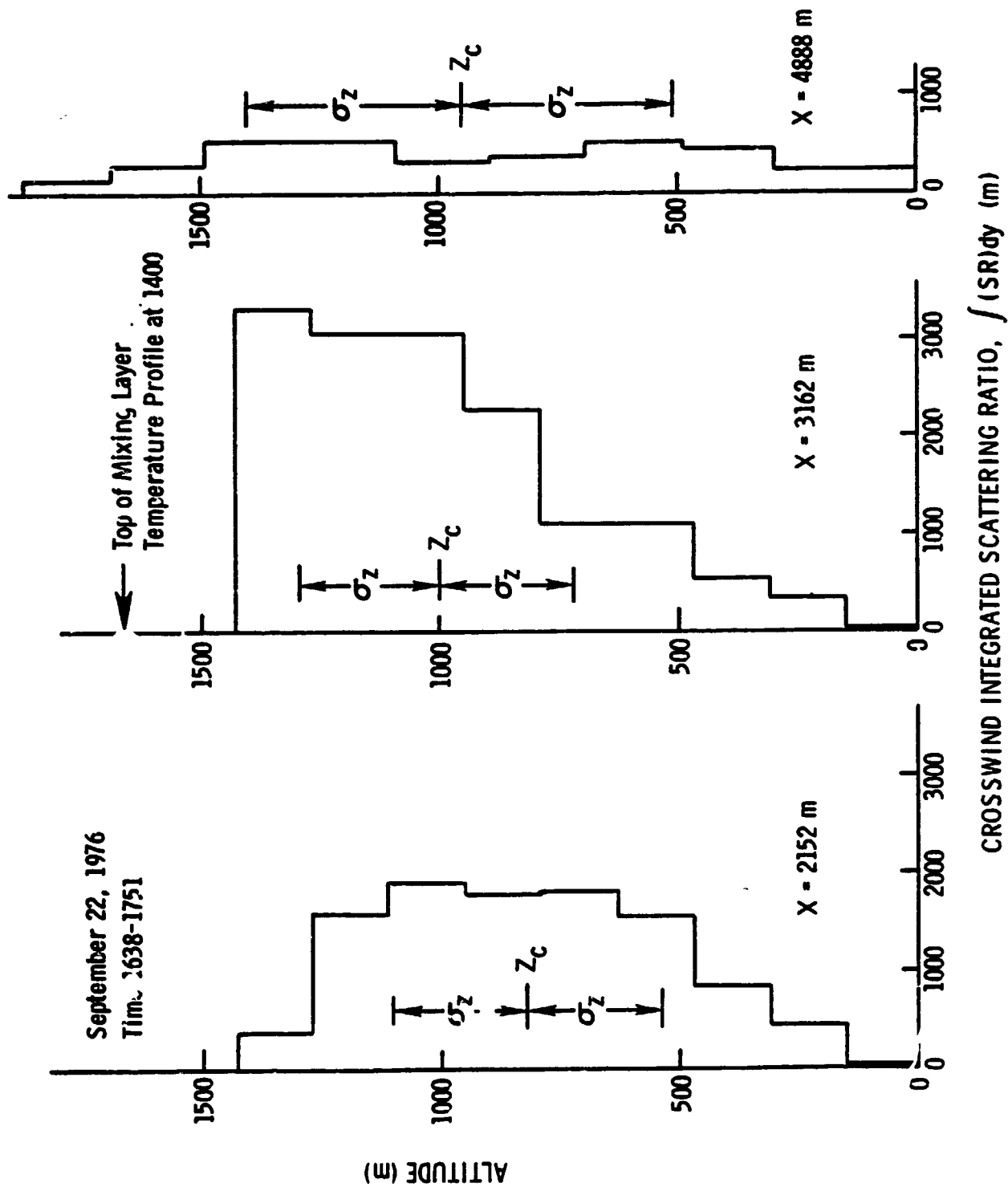
Figure 4. Average vertical profiles of crosswind integrated scattering ratio as a function of downwind distance. Z_c and σ_z are the centroid height and vertical standard deviation, respectively, of the measured distributions. (Measurements approximate hourly averaged profiles.)

Oct. 15, 1976
1142 - 1158
x = 1142 m

——— Scattering Ratio

- - - SO_2

ELEVATION ANGLE (deg)

20

10

0

NORMALIZED INTEGRATED CONCENTRATION ALONG INSTRUMENT LINE OF SIGHT, $\int cd\eta \, / \, [\int cd\eta]_{max}$

0.5

1.0
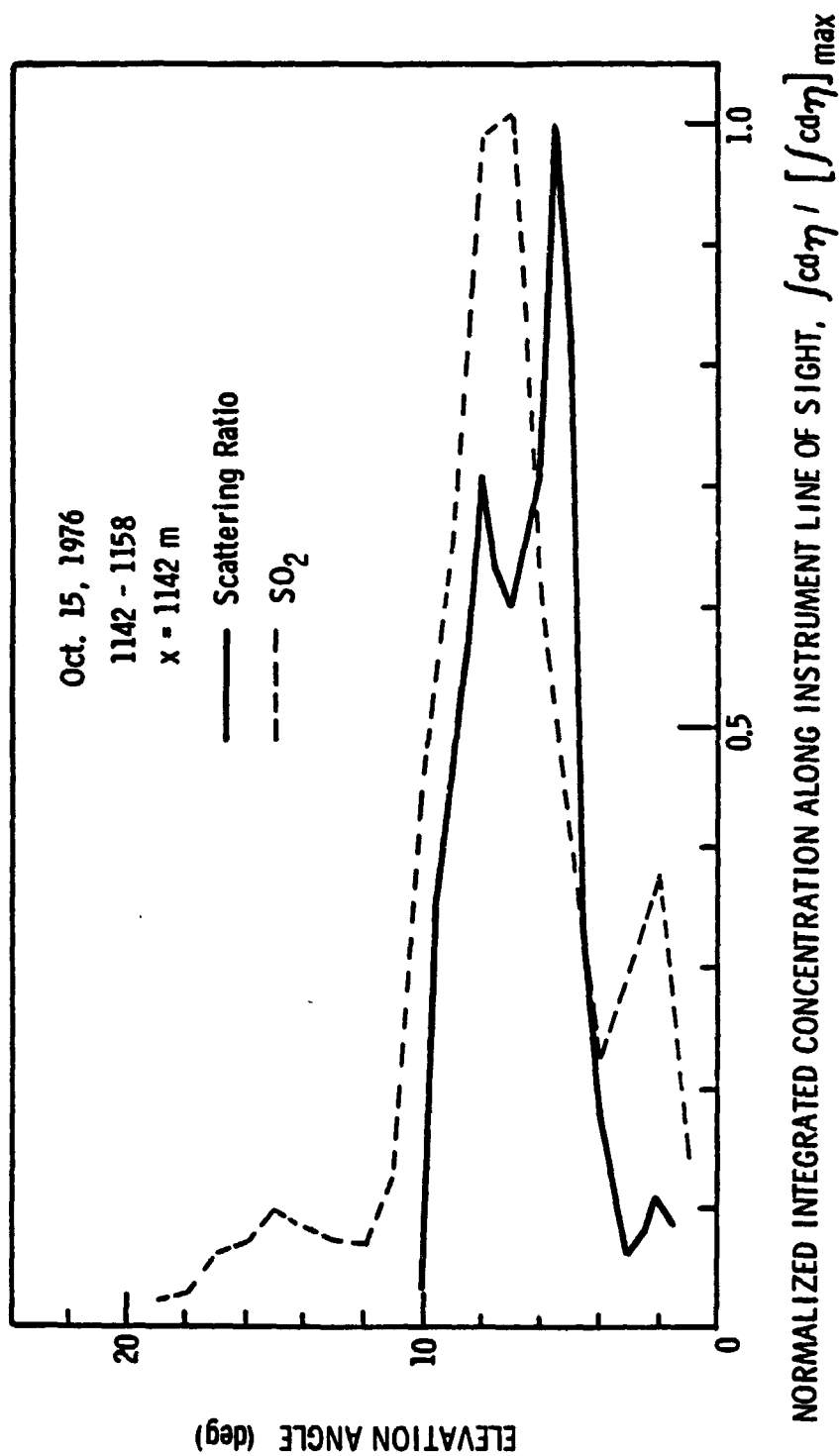
Figure 5. Average integrated SO_2 concentration and scattering ratio as a function of elevation angle.

III. PLUME RISE

This section is divided into two parts. In part A, observations of the initial plume rise are compared to predictions from the "two-thirds law." The main purposes of these comparisons are to determine if plume rise enhancement occurs when two adjacent stacks, rather than one stack, are operating, and to determine the proportionality constants between measured dispersion (or plume radius) and plume rise. These constants are used in Section IV.A. In part B, formulas for the final rise in neutral and convective atmospheric conditions are tested against observations of final rise. The formulas tested are Briggs (1970) model for neutral conditions, Weil's (1974) modification to it to account for convective turbulence, and Briggs (1975) models which include one formula for neutral, high wind conditions and two for convective conditions.

A. Initial Rise - the "Two-Thirds Law"

The initial rise of a buoyant plume in a neutral atmosphere and in the presence of a crosswind can be predicted by the "two-thirds law" (Briggs, 1975), which predicts that plume rise z increases with downwind distance x according to

$$z = \left(\frac{3}{2\beta^2}\right)^{1/3} \ell^{1/3} x^{2/3} \qquad (1)$$

where β = an empirical entrainment parameter

ℓ = buoyancy length scale given by

$$\ell = \frac{F}{v^3} \qquad (2)$$

where F = the buoyancy flux (defined in the Nomenclature)

v = average wind speed.

The model leading to equation (1) is based on uniform or "top hat" profiles of density, temperature, and velocity within a circular plume cross section of radius r. The radius is predicted to grow in proportion to the plume rise. If one chooses equivalent* Gaussian profiles to describe the variation of plume properties across the plume, the standard deviation of the Gaussian profile is $r/\sqrt{2}$.

Predictions of the "two-thirds law" are compared first to observations when only one stack was operating. Measured nondimensional plume trajectories shown in Fig. 6 are in good agreement with the prediction of equation (1) using the recommended β (0.60) given by Briggs (1975). If one exceptional trajectory is deleted (symbol +), the average β is 0.59. (A β was calculated for each individual point in Fig. 6 from equation (1) using the observed plume rise, distance x, and measured F and v. The average of these β's was 0.59.)

The discrepancy between the predicted and observed trajectory for the exceptional case is believed due to differences in wind speed measured from pibals and actually experienced by the plume. The measured wind profile showed an average speed over the mixing layer of ~ 6m/sec and an average direction of 10°**, indicating that air passed over land upwind of the plant. This profile was measured from a site about 1 km east of the plant (see Fig. 2). However, measured plume cross sections out to 2 km downwind of the stacks indicated that the wind direction was ~ 345°, i.e., blowing down the

---

* By equivalent, we mean that the volume, momentum, and buoyancy fluxes in the Gaussian profile formulation are the same as those with "top hat" profiles.

** Wind direction is that from which the wind blows, measured from north.
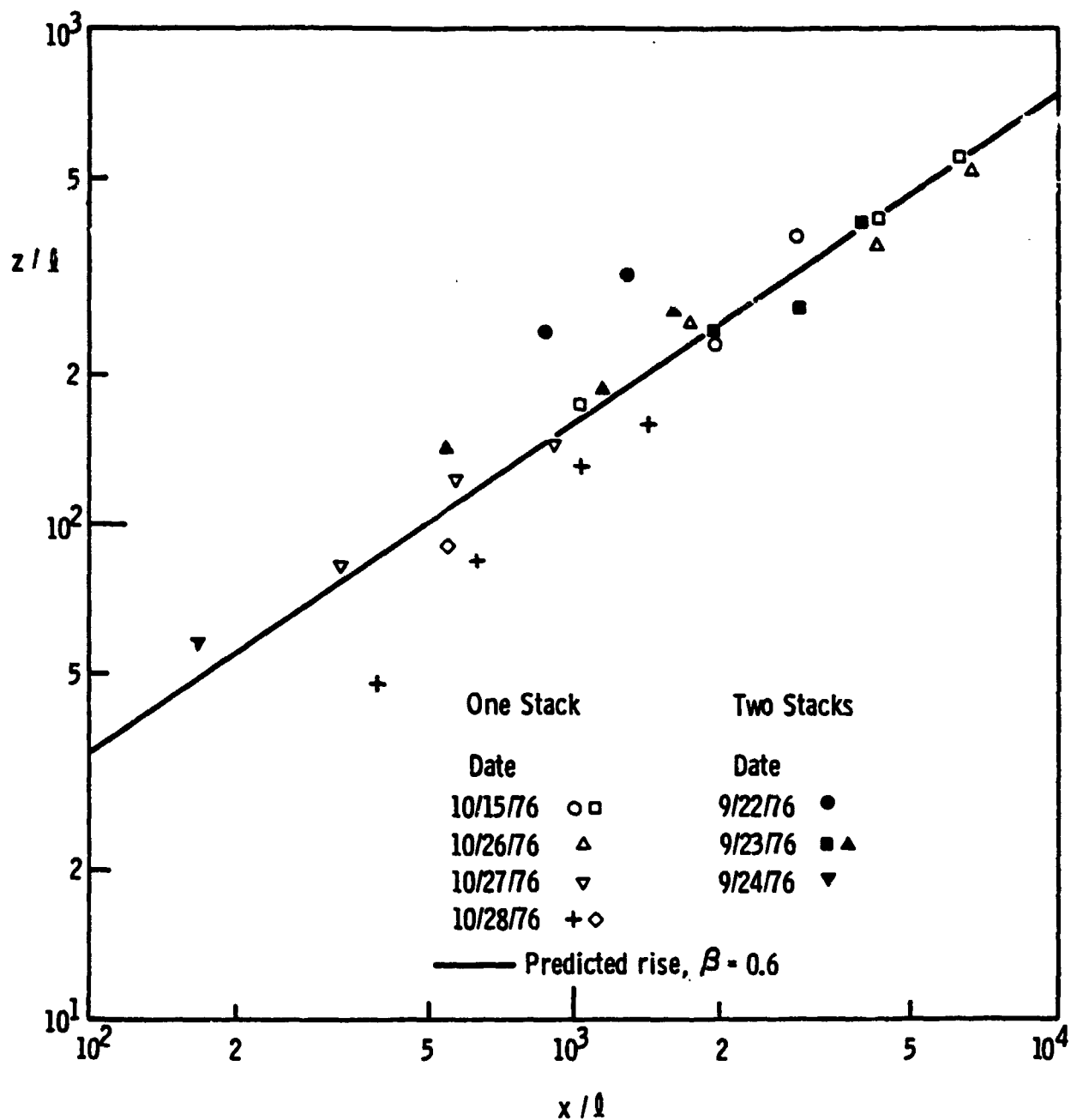
Figure 6. Comparison between plume rise prediction from "two-thirds law" (equation 1) and measured rise.

Martin Marietta Environmental Center

river. For winds coming down the river, the wind speed at plume elevation could be considerably higher than that measured at the pibal site because of the small roughness height over the water compared to that over land*, and the long fetch (~ 10 km) of water upwind of the plant. Higher winds would result in a lower plume rise, as observed.

Figure 7 shows a linear relationship between the observed vertical dispersion and the observed rise for the single stack data (solid line, open symbols). The average value of $\beta_{zE} = \sigma_z/z$ for the single stack data was 0.62; σ_z in Fig. 7 was computed from the average scattering ratio profile. The average instantaneous vertical dispersion from repeated scans $\langle\sigma_z\rangle$ also varied linearly with plume rise; the mean $\langle\sigma_z\rangle/z$ was 0.56. The equivalent "top hat" radii ($r = \sqrt{2}\,\sigma_z$) computed from the observed σ_z's were a greater fraction of the observed rise ($r/z \doteq 0.84$) than the value reported by Briggs (1975) ($r/z = 0.5$). This should be expected since Briggs' value was based on the visible half-width (from photographs) of rising plumes. (If the visible half-width is interpreted as one standard deviation, σ_z, then Briggs' observations are consistent with the present ones.)

The average instantaneous crosswind dispersion, $\langle\sigma_y\rangle$, was expected to be approximately equal to the vertical dispersion $\langle\sigma_z\rangle$. Although $\langle\sigma_y\rangle$ varied approximately linearly with rise, the mean $\langle\sigma_y\rangle/z$ (=0.92) was larger than the mean $\langle\sigma_z\rangle/z$. The $\langle\sigma_y\rangle$'s were exceptionally large due to low-level tails on the crosswind scattering ratio profiles. We suspect that these tails were an artifact possibly because of low signal-to-noise ratio caused by limiting lidar sensitivity, low particulate emission rate (~ 0.018 kg/sec) during the single stack observations, and/or the method of

---

* The land fetch consisted of open crop fields and wooded areas.
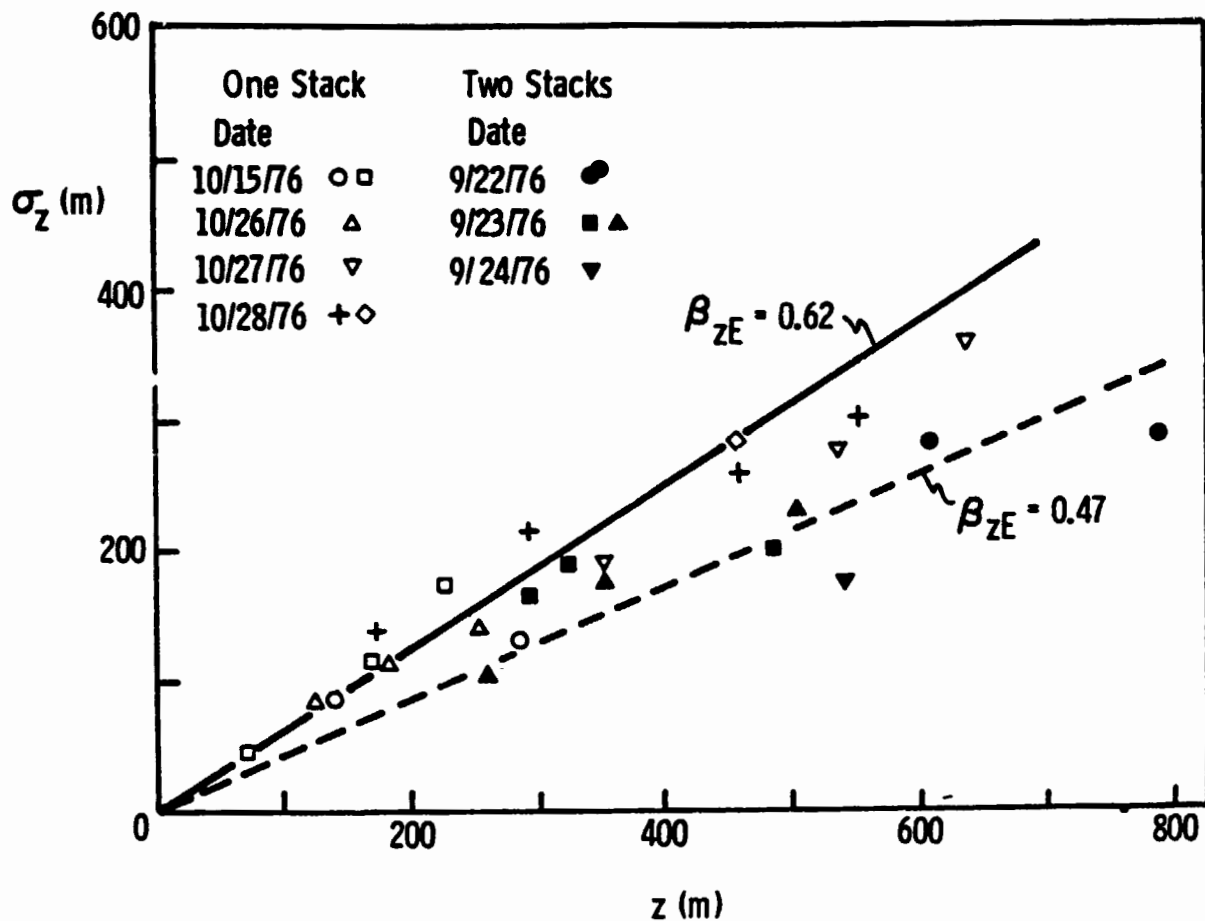
Figure 7. Measured vertical dispersion from average profiles as a function of measured plume rise. Solid and dashed lines are best fits of equation of form $\sigma_z = \beta_{zE} z$ to the single- and two-stack data, respectively.

Martin Marietta Environmental Center

determining backscattered light intensity in the plume's absence. Such tails were not found for the two-stack plume observations where the particulate emission rate was about a factor of 15 larger. We feel that in the absence of the low-level tails $\langle\sigma_y\rangle$ would be approximately equal to $\langle\sigma_z\rangle$ as was found for the two stack plume observations discussed below. This supposition and the sensitivity of $\langle\sigma_y\rangle$ to the low-level tails require further scrutiny.

Now consider lidar data taken with two stacks operating. For the most part, the plume rise measurements shown in Fig. 6 (closed symbols) exhibit a rise enhancement; i.e. the closed symbols lie along or above the upper edge of the scatter band of the single stack plume data. The only trajectory which does not show enhanced rise (symbol ■) was observed in the presence of a pronounced wind direction shear (= 0.035°/m). We believe that the directional shear caused a more rapid entrainment* of ambient air by the plume and that the increased entrainment resulted in a lower plume rise. If this exceptional case is deleted, the plume rises are close to the values obtained by using the sum of the buoyancy fluxes in the "two-thirds law."** For two nearby stacks of equal buoyancy flux as in the present observations, the predicted rise with two stacks operating is 1.26 times the rise with only one stack operating.

---

* The ratio σ_y/z for the exceptional trajectory ranged from 0.64 to 0.86 vs the mean of 0.47 for the nonexceptional cases (two stacks operating).

** For the two-stack cases, the mean value of $C = (1.5/\beta^2)^{1/3}$ (equation 1) determined from the six nonexceptional data points is 2.20; the standard deviation is 0.42. For the single stack cases, the mean C computed from 12 nonexceptional points is 1.64, and the standard deviation is 0.17. The ratio of the two means is 1.34; the ratio computed by assuming full plume merging is 1.26. The difference between the mean C's for two- and single stack cases is significant by a "Student t" test at the 99 percent confidence level.

The average σ_z/z of 0.47 found for the two stack cases in Fig. 7 is less than that for the single stack cases. This difference implies that the internal dynamics for the two-stack plumes are not the same as those for a plume emitted from one stack with a buoyancy flux of 2F, even though the observed plume rise implies otherwise. Most of these measurements were obtained between 2 km and 3 km downwind of the stacks. Since standard deviations were typically 2-1/2 to 3 times the distance between the stacks, a considerable overlap of the two individual plumes should have occurred. The mean ratios of $\langle\sigma_z\rangle/z$ and $\langle\sigma_y\rangle/z$ for the two stack cases were about 0.35.

To develop a generalized treatment for two stack plumes, further investigation is required of the distance and wind direction dependence of the plume rise and growth (wind direction relative to the line of stack centers). The growth rate should depend on the plume's internal circulation, which has not yet been explored for a two-stack plume. The two-stack plumes observed here suggest that travel distances beyond those measured here are required for evolution into the single double-vortex structure characteristic of a single stack plume. Detailed observations of the internal circulation could probably best be obtained from simulations in a wind tunnel or water channel. Wind tunnel simulations of plume rise from two adjacent stacks are presently being conducted for the Maryland Power Plant Siting Program.*

Crosswind dispersion from the average profile was larger than the associated vertical dispersion, presumably due to lateral plume meandering, which is not taken into account in the entrainment model. This meandering is dealt with in Section IV.

---

* Dr. T' mas J. Overcamp, Environmental Systems Engineering Department, Clemson University, Clemson, South Carolina.

Martin Marietta Environmental Center

B. Final Rise Formulas - Neutral and Unstable Conditions

Several extensions of the "two-thirds law" have been formulated by Briggs (1970, 1975) to predict the final rise of buoyant plumes in neutral and unstable conditions. In earlier work, Briggs (1970) proposed that, in neutral conditions, plume growth due to buoyancy-generated turbulence would, at some downwind distance, be replaced by growth caused by atmospheric turbulence, and the latter would cause more rapid dispersion and a limited rise. He suggested the following formula for computing the final rise in such conditions:

$$\Delta h = 1.6 \ell^{1/3} (3.5x^*)^{2/3} \tag{3}$$

where x^* is the distance of transition from growth due to buoyancy-generated turbulence to that caused by atmospheric turbulence and is given by

$$
\begin{aligned}
x^* &= 14 \ F^{5/8} & F &< 55 \ m^4/sec^3 \\
x^* &= 34 \ F^{2/5} & F &> 55 \ m^4/sec^3 \ .
\end{aligned}
\tag{4}
$$

To arrive at these expressions for x^*, Briggs utilized an empirical formula for the ambient turbulent dissipation rate ϵ during neutral stability.

Weil (1974) suggested a modification to this model to predict a final rise caused by convective turbulence during unstable ambient conditions. He proposed that the ambient turbulent dissipation rate for convective conditions could be given by

$$\epsilon = 0.5q \tag{5}$$

where

$$q = \frac{gQ_o}{\rho c_p T} \tag{6}$$

where g = acceleration due to gravity

Q_o = sensible heat flux at the surface

ρ = air density

T = absolute temperature

c_p = specific heat at constant pressure.

(ρ, T, and c_p are evaluated at the surface.) The resultant formula for
x* is

$$x^* = 0.65 \; \frac{F^{2/5} v^{3/5}}{q^{3/5}} \qquad (7)$$

in which Weil assumes Q_o = 0.31 times the insolation rate. In calculating
a final rise for ground-level concentration predictions during neutral or
unstable conditions, Weil (1974, 1977) chose the lower of the estimates for
x* given by equations (4) and (7). This procedure was used to estimate the
highest ground-level concentrations and to avoid the difficulty in distin-
guishing neutral from convective conditions, solely on the basis of measured
lapse rates at plume altitudes. Furthermore, this approach produced the best
agreement between measured and calculated concentrations.

In his more recent work, Briggs (1975) proposed two new models for
computing the final rise. The first assumes that plume "break up" and final
rise occur when the turbulent dissipation rate inside the plume decays to
the dissipation rate of the surrounding turbulent environment. The dissi-
pation rate inside the plume is based on simple dimensional arguments using
the "two-thirds law" while the atmospheric dissipation rate is based on
classical results for the neutral surface layer and the convective mixing
layer.

For neutral high wind conditions in which mechanical turbulence is
likely to be responsible for plume "break up," Briggs assumes

Martin Marietta Environmental Center

$$\epsilon = \frac{u_*^3}{\kappa h} \tag{8}$$

where $u_* =$ friction velocity

$\kappa =$ von Karman constant (≈ 0.4)

$h =$ height above ground.

The final rise is then

$$\Delta h = 1.3 \left(\frac{F}{vu_*^2}\right)\left(1 + \frac{h_s}{\Delta h}\right)^{2/3} \tag{9}$$

where $h_s =$ stack height. Equation (9) can be solved iteratively for the final rise Δh. The friction velocity was estimated here as some fraction of the mean wind speed. We found that $u_* = v/16$ provides good agreement between measured and observed plume rise.

For plumes rising in convective mixing layers, Briggs argues that downdrafts are responsible for terminating rise, and that the dissipation rate within the downdrafts should be used in determining final rise. He suggests $\epsilon \simeq 0.1q$ for the downdrafts with the resulting formula:

$$\Delta h = 4.3 \left(\frac{F}{v}\right)^{3/5} q^{-2/5} \quad . \tag{10}$$

Briggs assumes $Q_0 = 0.4$ times the solar insolation rate.

The second new model posed by Briggs -- the "touchdown" model -- treats the case of plumes brought to ground by downdrafts during strong convection. This model differs from the "break up" model in that the plume is assumed to still be rising relative to the air in a convective downdraft, but the velocity of the downdraft exceeds the rise velocity of the plume. The formula for final rise is

$$\Delta h = 1.0 \left(\frac{F}{vw_d^2} \right) \left(1 + \frac{2h_s}{\Delta h} \right)^2 \qquad (11)$$

where w_d = the constant downward velocity of the downdraft

$$w_d = 0.4 \ (qH_m)^{1/3} \qquad (12)$$

in which H_m = the mixing depth. Equation (11) can be solved iteratively for the final rise.

In the comparisons below, plume rise limited by the inversion capping the mixing layer was also considered. The net plume rise plus some fraction of σ_z was assumed equal to the distance between stack top and the top of the mixing layer. The fraction was empirically found to be 1, resulting in the formula

$$\Delta h = \frac{H_m - h_s}{1 + \beta_{zE}} \quad . \qquad (13)$$

(It is assumed that the relationship $\sigma_z = \beta_{zE} z$ holds until the final rise is reached.)

The final rise from measured plume trajectories was chosen as the maximum centerline rise provided that the maximum was not the most distant observation on the trajectory. The most distant measurement was not considered as a "final rise" because further rise may have occurred beyond that point if the plume were still rising. A final rise was found on seven of 11 plume trajectories*;

---

* One exception to the final rise criterion was made for a trajectory measured on September 22, 1976 (time 1559-1619). Only one cross section was scanned, but the measured plume rise was 34 percent lower than the "two-thirds law" prediction; the cross section was about 3200 m downwind of the stacks. The plume measurement was judged to be one of final rise and correlated well with the neutral "break up" model prediction (see Table 2).

Martin Marietta Environmental Center

Table 2. Comparison between maximum observed plume rises and final rise predictions.

Observation Group	Date	Stacks Operating	Time	x (m)	Δh_meas	v (m/sec)	H_m (m)	$\Delta h_{meas}/\Delta h_{pred}$ Briggs (1970) Neutral Eqs.(3),(4)	Briggs (1970) Convective Eqs.(5),(7)	Briggs (1975) Breakup Neutral Eqn.(9)	Briggs (1975) Breakup Convective Eqn.(10)	Briggs (1975) Touchdown Eqn.(11)	Inversion limited Eqn.(13)
1. Final rise observed; turbulence limited	9/22/76	2	1559-1619	3210	192	13.7	1650	1.03*	0.60	0.92*	0.43	0.43	0.20
	9/22/76	2	1638-1751	3162	792	6.7	1650	2.06	1.32	0.66	0.94	1.04	0.81
	10/26/76	1	1700-1810	3207	254	11.9	1250	1.40	0.40	1.02	0.29	0.28	0.40
2. Final rise limited by inversion	9/24/76	2	1253-1342	2527	657	4.3	1100	1.11	0.97	0.16	0.70	0.66	1.09
	10/15/76	1	1217-1236	2114	286	10.0	700	1.40	1.03	0.83	0.74	0.56	0.95
	10/27/76	1	1433-1614	3941	636	5.8	1250	1.67	1.08	0.40	0.78	0.77	0.95
	10/28/76	1	1025-1154	4951	553	6.2	1100	1.57	1.23	0.42	0.88	0.83	1.01
3. Final rise not observed; maximum plume rise is most distant observation on trajectory	9/23/76	2	1337-1412	4564	485	8.4	1200	1.63	1.27	0.76	0.91	0.84	0.72
	9/23/76	2	1529-1608	2979	502	7.3	1200	1.45	1.03	0.54	0.74	0.71	0.75
	10/15/76	1	1354-1501	2506	225	12.1	1200	1.36	.88	1.04	0.53	0.58	0.37
	10/28/76	1	1516-1632	2682	456	5.5	1200	1.15	0.52	0.25	0.59	0.58	0.75

* For each group of formulas, Briggs (1970) and Briggs (1975), the $\Delta h_{meas}/\Delta h_{pred}$ ratio for the formula predicting the lowest rise is underlined.

the maximum rise of the remaining four trajectories was the most distant observation. The maximum rises were divided into three groups:

1. Final rise was observed and was caused by turbulence (i.e., rise not limited by capping inversion); three cases.

2. Final rise was observed but was caused by an upper level inversion (these observations correlated quite well with equation 13); four cases.

3. Final rise was not observed. Maximum plume rise measured was the most distant observation on a given trajectory; four cases.

Although the last two categories cannot be used to verify formulas for turbulence limited rise, they can be used to show that a particular model does not apply (i.e., the observed plume rise is greater than that predicted by that model).

Comparisons between measured and predicted plume rises are summarized in Table 2. In each group of formulas, Briggs (1970) and Briggs (1975), we choose the one giving the lowest rise as the formula to be used in calculating the final rise and effective stack height. This choice is made for the reasons given by Weil (1974, 1977) and discussed earlier. In Table 2, underlining denotes the ratio of predicted to observed rise for the formula giving the lowest rise. The Briggs (1970) model does not correlate well with observations. The neutral rise prediction, equations (3) and (4), gives lower estimates of rise than the formula for convective conditions, equations (3) and (7), in all cases. It also underestimates the maximum measured rise in all three groups of observations. The failure of the 1970 neutral rise prediction is not unexpected in view of the result in Fig. 7 showing a linear dependence of plume growth on rise; the Briggs (1970) model predicts a faster than linear growth rate beyond the distance x*, a prediction not supported by observations.

The Briggs (1975) models provide good agreement with the three observations of turbulence-limited rise. The 1975 formulas are also consistent with

Martin Marietta Environmental Center

the maximum measured rises in groups 2 and 3 (Table 2); predicted rise is either greater than or approximately equal to the observed rise. Note that inversion-limited rises (group 2) correlate well with equation (13) (last column of Table 2).

The predicted final rise for cases with two stacks operating was obtained by multiplying the calculated final rise for one stack by $2^{1/3}$. This is consistent with the "two-thirds law" applied at the distance of final rise for a single stack plume. Although we might be tempted to use summed buoyancy fluxes in the final rise formulas*, the observed plume growth in the "two-thirds law" regime (Fig. 7) does not indicate that the local plume geometry, or probably internal dynamics, for the two-stack plume is the same as that for a plume emitted from one stack with buoyancy flux 2F. The approach used here for computing final rise seems most prudent until further observations indicate otherwise.

---

* This could lead to predicted final rises for the two-stack plume of $2^{0.6}$ times the final rise for a single stack plume.

IV. DISPERSION ESTIMATES AND GROUND-LEVEL SO$_2$ CONCENTRATIONS

A. Free Convection Scaling and the "Two-Thirds Law"

Deardorff's (1972) numerical modeling of the convective mixing layer showed that large convective eddies scale in size with H$_m$ while turbulent velocities within this layer vary with the convective velocity scale w$_*$, given by

$$w_* = (qH_m)^{1/3} .$$
(14)

The appropriateness of H$_m$ and w$_*$ as the important length and velocity scales during strong convection was supported by laboratory simulations of turbulence in a water-filled convection chamber (Willis and Deardorff, 1974), wherein good agreement was found between these laboratory measurements and atmospheric observations. Recently, the convection chamber was used to simulate dispersion of neutrally buoyant particles into the mixed layer from a point source at a height of 0.25H$_m$ (Willis and Deardorff, 1978). The nondimensional plume standard deviations, σ_y/H_m and σ_z/H_m, were given as functions of a nondimensional distance X, where

$$X = \frac{w_*}{v} \frac{x}{H_m}$$
(15)

i.e., the travel time x/v divided by H$_m$/w$_*$, a characteristic time scale for convective eddies in the mixed layer.

Lamb (1978a) conducted numerical simulations of neutrally buoyant particle diffusion from a point source into the mixed layer using the turbulence

Martin Marietta Environmental Center

velocity fields computed numerically by Deardorff (1974). The simulations for a source height of $0.26H_m$ were in excellent agreement with the laboratory results of Willis and Deardorff (1978). In a more recent paper, Lamb (1978b) investigated the dispersion characteristics for higher point source releases, at $0.5H_m$ and $0.75H_m$, and summarized his results into a simplified set of expressions. For release heights greater than $0.1H_m$, Lamb gave

$$\frac{\sigma_y}{H_m} = \begin{cases} \frac{1}{3} X, & \text{for } X < 1 \quad\quad (16a) \\[2ex] \frac{1}{3} X^{2/3}, & \text{for } 1 < X \leq 3 \quad\quad (16b) \end{cases}$$

$$\frac{\sigma_z}{H_m} = \begin{cases} \frac{1}{2} X, & \text{for } X < 2/3 \quad\quad (17a) \\[2ex] \frac{1}{3}, & \text{for } X > 2/3 \quad\quad (17b) \end{cases}$$

These results apply for v/w_* in the range

$$1.2 \leq \frac{v}{w_*} \leq 6.0 \quad . \quad\quad\quad (18)$$

The lower limit is imposed to ensure that diffusion along the plume axis can be ignored while the upper limit satisfies the condition that the bulk of the mixing layer be dominated by convective turbulence. (See Lamb, 1978b, for σ_y and σ_z expressions applicable to release heights less than $0.1H_m$.)

In the case of a buoyant stack plume dispersing in a convective mixing layer, we expect the plume standard deviations to be given by equations (16) and (17) far from the stack, where there are no longer stack buoyancy effects. Close to the stack, buoyancy-induced growth and rise should dominate the plume behavior. However, even near the stack, lateral meandering of the plume needs to be considered to predict σ_y for the time averaged plume.

The crosswind dispersion of a time averaged plume can be represented as

$$\sigma_y = (s_y^2 + m_y^2)^{1/2} \qquad (19)$$

where s_y is the "relative" dispersion about the instantaneous plume center-line and m_y is the "meandering" of the centerline about its time averaged position (see Csanady, 1973). Close to the source s_y and m_y can be of the same order of magnitude while far from the source $s_y \gg m_y$. By "near" we mean for travel times $x/v < t_L$, where t_L is the Lagrangian integral time scale and by "far", we mean $x/v \gg t_L$. In a convective mixing layer $t_L \sim H_m/w^*$, and the travel time separating "near" and "far" is $x/v \sim H_m/w^*$ which is equivalent to $X \sim 1$.

Now consider buoyant plume dispersion in the region $X \leq 1$. We assume that the principal contribution to the "relative" dispersion is buoyancy-induced entrainment, and we have

$$s_y = \beta_{yL} z \qquad (20)$$

where β_{yL} = the mean $\langle \sigma_y \rangle /z$ found earlier*

    z = the rise above the stack.

Equation (20) should hold until the final rise Δh is reached. For distances beyond that to final rise, we assume that $s_y = \beta_{yL} \Delta h$. The "meandering" component of the dispersion, m_y, ought to vary linearly with travel time or distance for $X < 1$ according to statistical theory of turbulence (Taylor, 1921).

---

* For single stack plumes, we assumed $\beta_{yL} = 0.56$, which was the mean value found for $\langle \sigma_z \rangle /z$. This assumption was made because the calculated $\langle \sigma_y \rangle$'s were believed to be unrealistically large due to artificial low-level tails on the crosswind scattering ratio profile. (See discussion in Section III.A.) For the two-stack plumes, $\beta_{yL} = 0.35$.

        Martin Marietta Environmental Center

Since Lamb's result (equation 16a) is consistent with statistical theory, we assume it to be representative of m_y for $X \leq 1$. The "total" dispersion can then be computed from equation (19) by replacing s_y by $\beta_{yL} z$ and m_y by $1/3\ X$.

For dispersion in the region $X > 1$, we do not attempt to resolve the dispersion into "relative" and "meandering" components. In this region we are guided by the idea that σ_y should tend asymptotically to $1/3\ X^{2/3}$ (equation 16b), and that there should be a smooth transition of σ_y in $X < 1$ to σ_y in $X > 1$. We also note that for strongly buoyant plumes which are still rising for $X > 1$, buoyancy-induced entrainment will continue to contribute to the "total" σ_y.

Consistent with the above discussion, the following formula is proposed for computing σ_y:

$$
\frac{\sigma_y}{H_m} = \begin{cases} \left[2.6\ \beta_{yL}^2 \left(\dfrac{F}{v w_* ^2 H_m} \right)^{2/3} X^{4/3} + \dfrac{1}{9}\ X^2 \right]^{1/2} & , \text{ for } X \leq 1 \quad (21a) \\[4em] \left[2.6\ \beta_{yL}^2 \left(\dfrac{F}{v w_* ^2 H_m} \right)^{2/3} X^{4/3} + \dfrac{1}{9}\ X^{2/3} \right]^{1/2} & , \text{ for } 1 < X. \quad (21b) \end{cases}
$$

The first term within the brackets on the right hand side of equation (21) is $\beta_{yL}^2 z^2 / H_m^2$ in which z has been replaced by equation (1) to yield the $X^{4/3}$ dependence. The buoyancy-induced entrainment represented by this first term is assumed to increase only up until the final plume rise is reached. For $X \geq X_f$, where X_f is the nondimensional distance to final rise, the first term inside the brackets is assumed to be constant and evaluated at $X = X_f$. The second term inside the brackets is the square of the dispersion given by Lamb's

results (equation 16a is used for the second term in equation 21a and equation 16b for the second term in equation 21b). For two-stack operation, the sum of the buoyancy fluxes is used in equation (21).

Measured and predicted values of σ_y/H_m are in close agreement, as shown in Fig. 8. The solid lines are the average prediction curves (equation 21) for the different cases plotted and deviate from the individual curves (not shown) by less than 5 percent. Note that the solid curves differ from the Lamb prediction most significantly for $X < 1$, the region where plume rise and buoyancy-induced entrainment occur. For the cases shown, a typical distance to final plume rise is $X_f = 0.8$. Only cases meeting the criteria of equation (18) are used in this analysis.

Fig. 8 shows that the single stack data (Fig. 8a) tend to lie slightly above the solid curve, whereas the two-stack data (Fig. 8b) tend to lie somewhat below it. One possible explanation for these differences may be the different wind directions and surface heat transfer characteristics upwind of the stacks in the two situations. For the single stack data, the wind came from the north to north-northeast and the upwind fetch was a mixture of open fields and trees where we would expect strong convective activity during midday. This convective field would be transported some distance across the Potomac River before the cooler water surface, with its reduced surface (to air) heat flux, would diminish convective mixing. For the two-stack cases, the wind came either from the northwest or southwest and traversed a considerable stretch of water upwind of the plant. In this situation, we would expect reduced convective activity and a smaller w_* in the air approaching the power plant. This would lead to less lateral meandering and the smaller σ_y found in Fig. 8b.

The vertical plume standard deviation followed the prediction of the "two-thirds law" quite well out to the final rise distance (Fig. 7). For distances

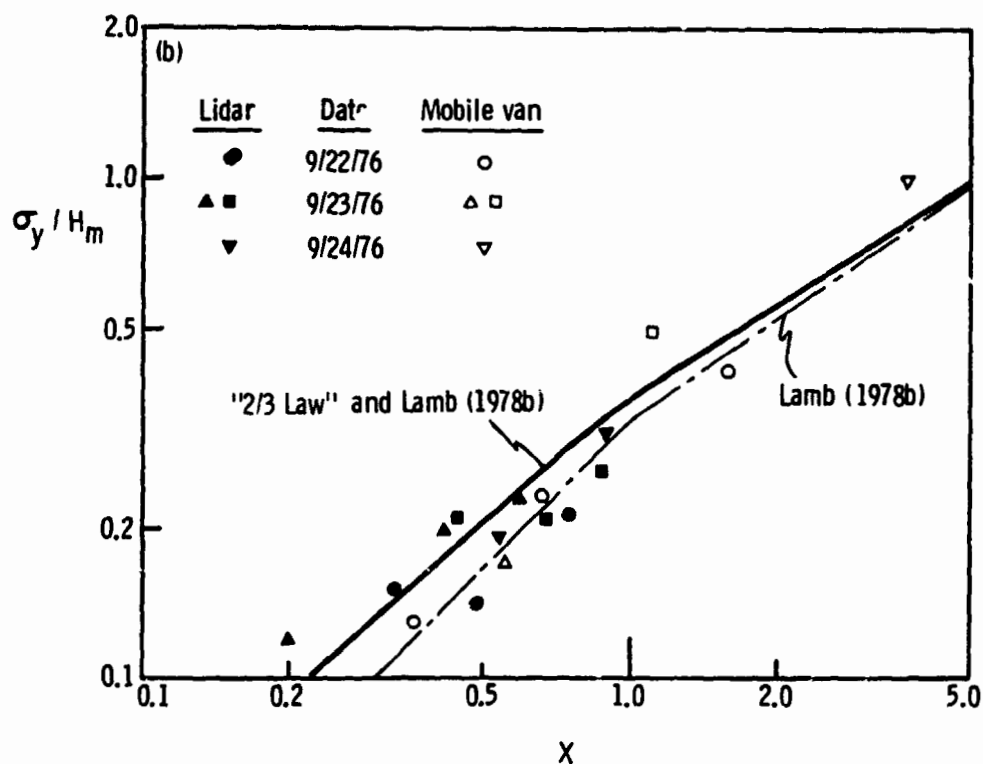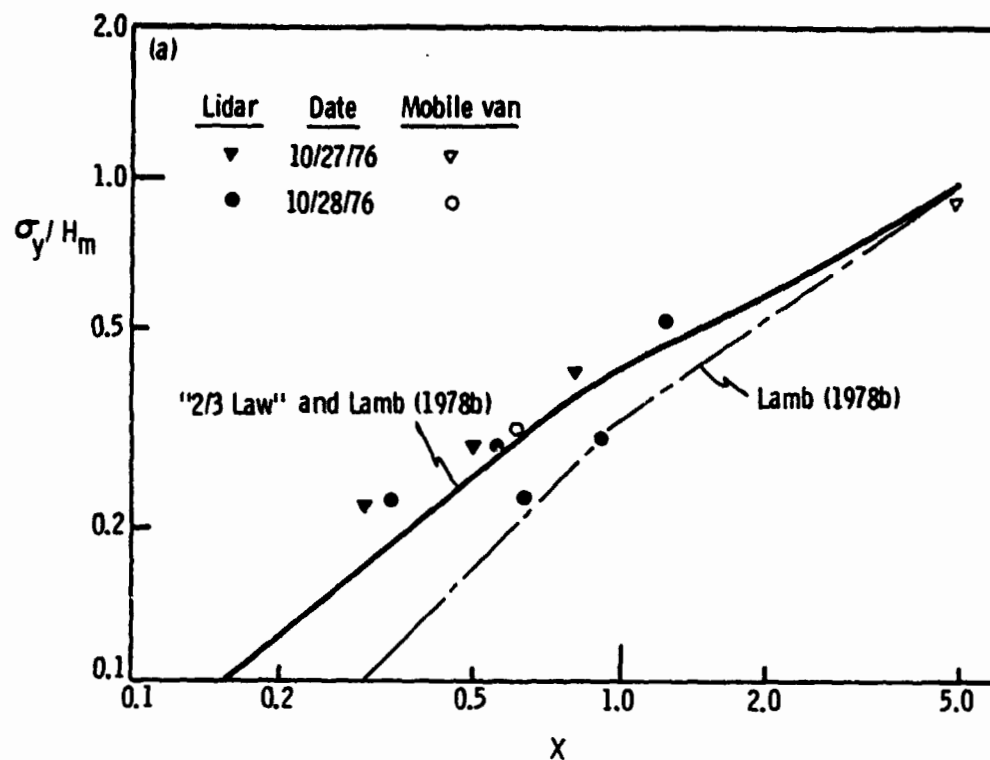**Martin Marietta Environmental Center**

Figure 8. Nondimensional crosswind standard deviation as a function of nondimensional downwind distance. Measurements compared to predictions using combined "two-thirds law" and Lamb (1978b) and Lamb's (1978b) numerical results. a) single stack cases; b) two-stack cases. (Measurements approximate σ_y of hourly averaged plume.)

beyond X_f, the plume should behave as a passive tracer, diffusing according to Lamb's results and with an initial σ_z (= σ_{zf}), given by the value at X_f. The linear vertical spread with distance (equation 17a) given by Lamb is a good approximation to his numerical results for source height releases of $0.25H_m$ and $0.50H_m$. However, for a release height of $0.75H_m$ and $X > 0.15$, Lamb's detailed results show a slower variation of σ_z with distance ($\sigma_z \propto X^{0.77}$) due to the lower velocities in downdrafts at the top of the mixing layer. This slower growth results in a 30 percent smaller σ_z than that given by equation (17) at $X = 2/3$.

From the above discussion, we propose a simple tentative formula for σ_z for $X > X_f$:

$$\sigma_z = \sigma_{zf} \left(\frac{X}{X_f} \right)^\gamma \quad , \qquad X > X_f \tag{22}$$

where $\gamma = 0.77$ and 1 for effective stack heights above and below $\sim 0.63H_m$, respectively. (For $X < X_f$, $\sigma_z = \beta_{zE} z$.) Equation (22) should hold only until the plume becomes uniformly distributed in the mixing layer. The limiting σ_z for a source at height h_e, is very far downstream,

$$\sigma_z = \left(\frac{1}{3} H_m^2 - h_e H_m + h_e^2 \right)^{1/2} \quad . \tag{23}$$

Lamb's approximate value for the limiting σ_z (= $1/3 H_m$) only differs by 15 percent from that given by equation (23) for h_e's between $0.25H_m$ and $0.75H_m$.

Only five data points were taken beyond the final rise distance for comparison to the σ_z prediction given by equation (22). These are shown in Fig. 9 along with other σ_z measurements made during the same time interval but at distances less than X_f. Predictions given by the "two-thirds law"

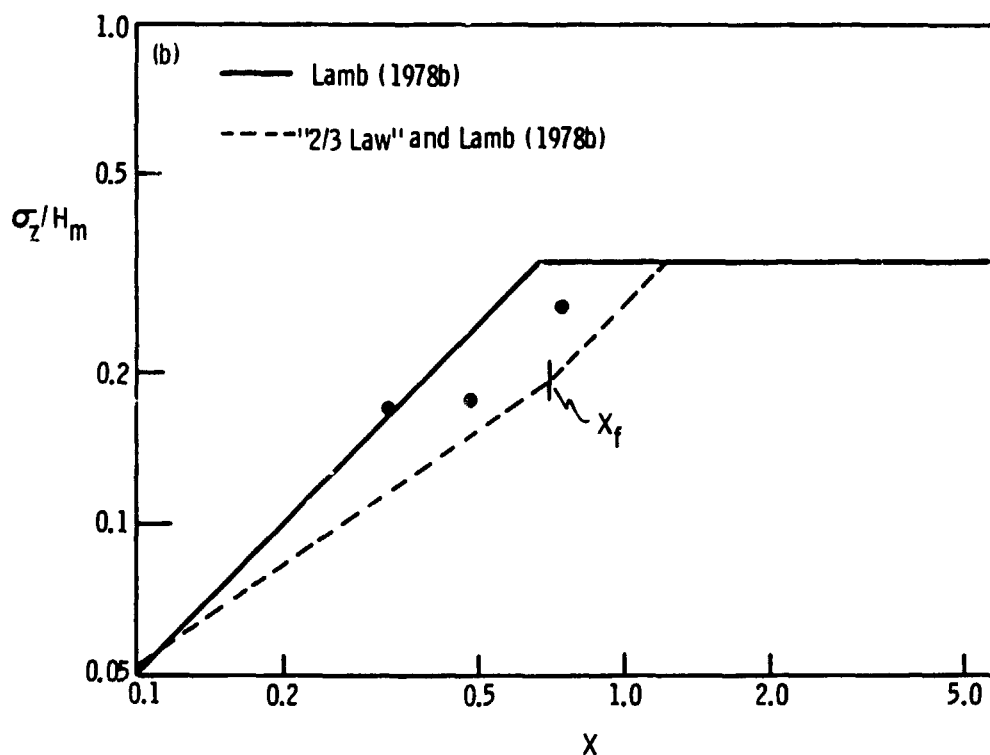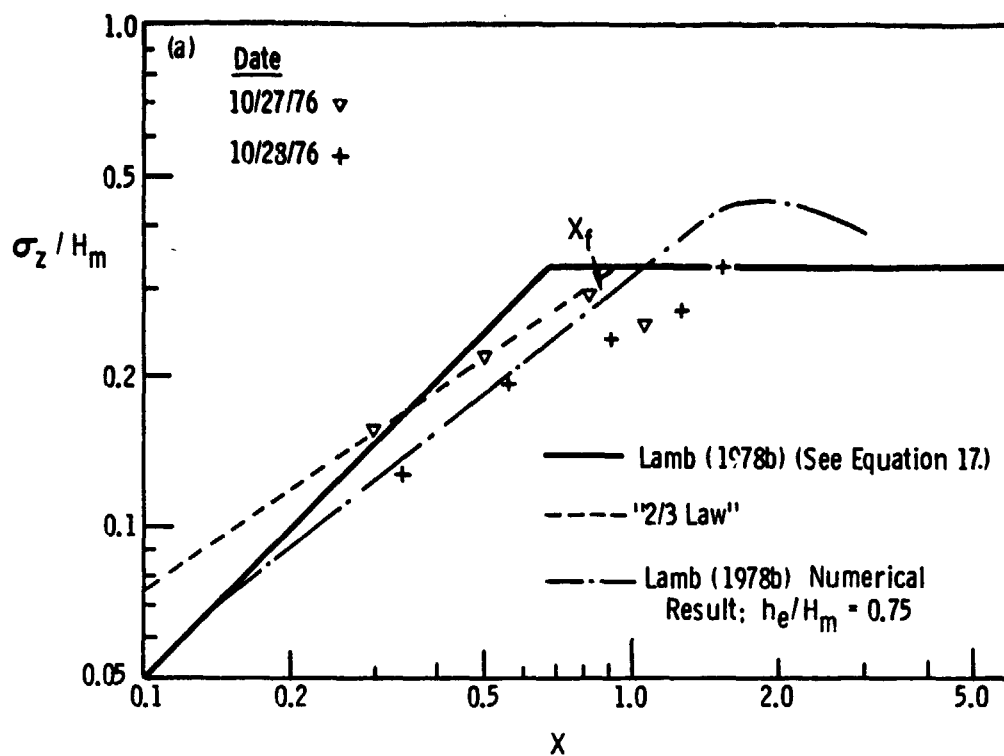**Martin Marietta Environmental Center**

Figure 9. Nondimensional vertical plume standard deviation as a function of nondimensional downwind distance. Measurements compared to predictions of "two-thirds law" and Lamb (1978b). a) single stack cases, h_e/H_m = 0.70; b) two-stack cases, h_e/H_m = 0.61. (Measurements approximate σ_z of hourly averaged plume.)

and equation (21) are shown out to X_f and beyond X_f, respectively. The data are in rough agreement with these predictions. Equation (17) (solid curve in Fig. 9) shows more rapid spreading than the "two-thirds law" prediction and generally predicts higher σ_z's than were observed. Lamb's numerical result (dash - dot curve) for $h_e/H_m = 0.75$ agrees roughly with the single stack data (Fig. 9a) where $h_e/H_m = 0.7$.

Two straightforward improvements in the σ_z prediction should be made. First, Lamb's σ_z should be resolved into the contribution due to vertical displacement of the plume centroid and that due to dispersion about the centroid. Only the latter contribution should be used in combination with the buoyant plume dispersion since vertical displacement of the buoyant plume centroid is treated separately by the rise formulas discussed earlier. (The data were not available in this study for the resolution of Lamb's σ_z into the above mentioned components.) Second, vertical meandering of the plume centroid during plume rise should be considered as a possible additional contribution to σ_z and treated as for σ_y. Although this was not necessary in the present analysis (in view of the good correlation in Fig. 7), the present data were collected when w_*/v was typically 0.25. For stronger convection where w_*/v might be 0.5 or greater, vertical meandering would play a more significant role in the time-averaged σ_z.

Calculations of ground-level SO_2 concentrations have been made using the Gaussian plume model with the above predicted σ_y and σ_z. To compute the effective stack height, we used the lowest plume rise given by the three following methods: the prediction of the "two-thirds law" at the measurement distance, the 1975 Briggs plume rise formulas (equations 9, 10, and 11), or the height of a trapped plume (equation 13). Calculated concentrations are compared to measured SO_2 values in Table 3. For the most part, the two are

Martin Marietta Environmental Center

Table 3. Comparison between calculated and observed ground-level SO$_2$ concentrations

Date	Time	x (m)	c$_{2~meas}$* (ppb)	"Two-Thirds Law" and Lamb		Brookhaven, Weil (1974) Algorithm				Pasquill, Turner (1964) Approach Drop 1 stability class				
				c$_{pred}$ (ppb)	$\frac{c_{pred}}{c_{2~meas}}$	Brookhaven Stability Class	c$_{pred}$ (ppb)	$\frac{c_{pred}}{c_{2~meas}}$	$\frac{x}{x_{max}}$	Pasquill Stability Class†	c$_{1~meas}$** (ppb)	c$_{pred}$ (ppb)	$\frac{c_{pred}}{c_{meas}}$	$\frac{x}{x_{max}}$
9/22/76	1047	2401	9	3	0.33	B$_1$	59	6.60	0.63	B	18	15	0.83	0.52
9/22/76	1359	8918	37	49	1.33	B$_1$	45	1.22	1.78	C	50	36	0.72	0.81
9/22/76	1645	4115	15	9	0.60	B$_1$	32	2.11	0.62	C	32	0.10	0.003	0.29
9/23/76	1320	5694	76	64	0.84	B$_1$	62	0.81	1.08	C	90	12	0.13	0.52
9/23/76	1524	3180	10	8	0.80	B$_1$	38	3.80	0.59	C	13	0.05	0.003	0.29
9/24/76	1154	12,271	45	105	2.33	B$_2$	49	1.10	4.02	A	63	56	0.89	7.48
10/27/76	1509	25,523	15	16	1.07	B$_1$	13	0.87	4.06	C	16	20	1.25	1.95
10/28/76	1607	3905	16	30	1.88	B$_1$	29	1.81	0.65	B	30	13	0.43	0.59

* c$_{2meas}$ = Maximum SO$_2$ concentration from average crosswind profile; approximately a 1-hour average.

** c$_{1meas}$ = Average of peak SO$_2$ concentration from repeated passes; approximately a 10-minute average.

† Pasquill stability class after the shift in stability condition.

in good agreement.* A summary of comparisons between measured and predicted σ_y, σ_z, and SO_2 concentrations is given in Table 4 (see "two-thirds law" and Lamb). Predictions based on free convection scaling and the "two-thirds law" agreed better with observations than those using empirical dispersion estimates (discussed below).

<div align="center">B. Empirical Dispersion Estimates</div>

Measured plume dispersion and SO_2 concentrations have also been compared to predictions based on the Brookhaven sigma curves using Weil's (1974) algorithm. The measured plume standard deviations are somewhat less than the Brookhaven B1 class predictions shown in Fig. 10 (see also summary in Table 4). Calculated ground-level concentrations using the Brookhaven dispersion estimates in the Gaussian model exceeded the measurements, on the average, by a factor of 1.76 (geometric mean). This is attributed to measurements made at distances less than x_{max}, the distance to maximum concentration. In four cases where $x \sim 0.6 \; x_{max}$ (Table 3), the geometric mean of c_{pred}/c_{meas} is 3.1 while the geometric mean of c_{pred}/c_{meas} for $x > x_{max}$ is 0.99. Concentrations close to the stacks were predicted to be higher than the observed because the vertical plume dispersion is overestimated.

Measured and calculated plume dispersions based on the Pasquill, Gifford, Turner (PGT) approach are compared in Fig. 11 for measurements falling in the neutral (Pasquill D) stability class. The PGT approach was tried both with the stability class selected for the prevailing meteorological conditions, and also with the next more unstable class. The σ_y predictions are in fair

---

* Predicted concentrations are within a factor of 2 of the measurements.

Martin Marietta Environmental Center
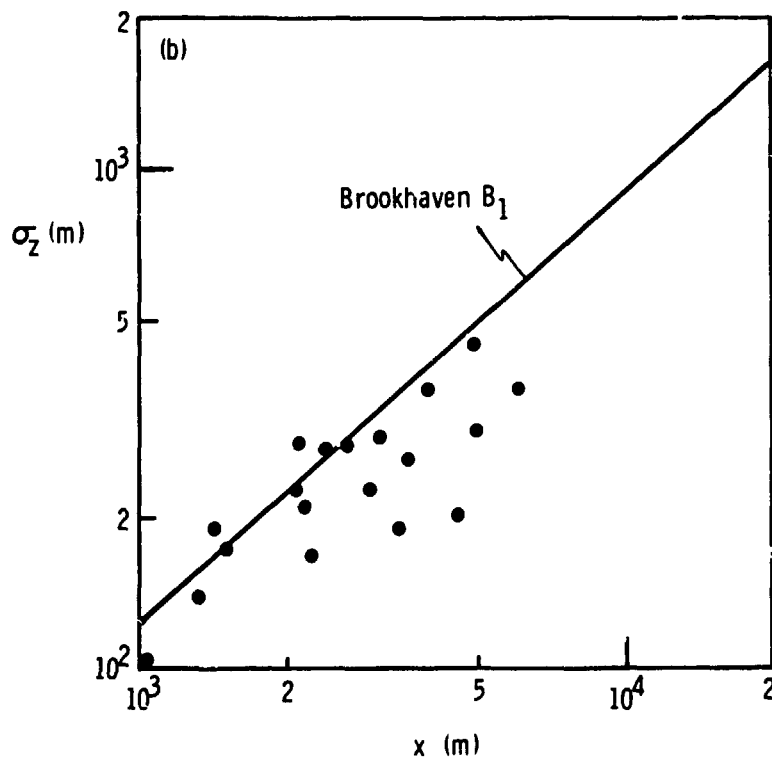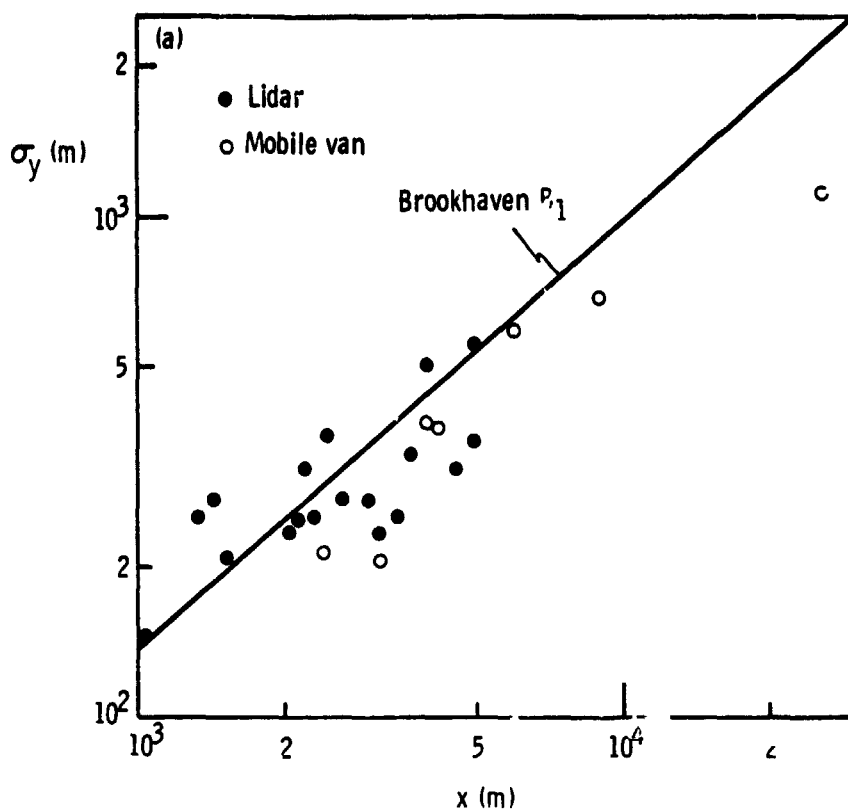
Figure 10. Measured plume standard deviations as a function of distance
compared to predictions of Brookhaven B_1 stability class;
stability class selected using Weil (1974) algorithm.
a) crosswind standard deviation; b) vertical standard deviation.
(Measurements approximate σ_y and σ_z of hourly averaged plume.)
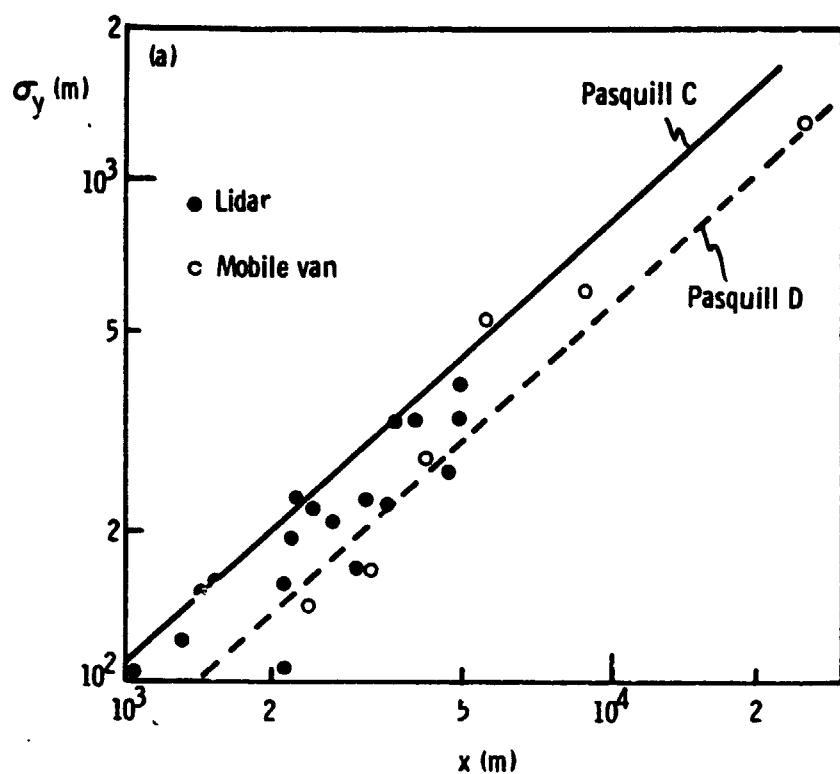
Figure 11. Measured plume standard deviations as a function of distance
compared to predictions of Pasquill-Gifford C and D sigma curves.
All measurements correspond to neutral (D class) stability as
determined by Turner (1964) approach. a) crosswind standard
deviation; b) vertical standard deviation. (Measurements
approximate σ_y and σ_z of 10-minute averaged plume.)

Martin Marietta Environmental Center

Table 4. Summary of comparisons between observed and calculated σ_y, σ_z, and ground-level SO_2 concentrations

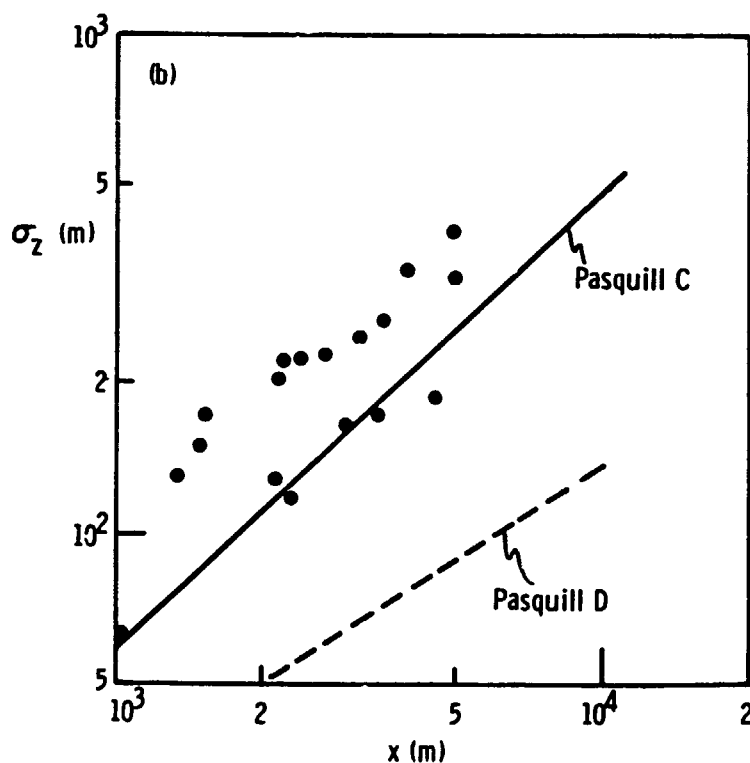| Ratio	"Two-Thirds Law" and Lamb	Brookhaven-Weil (1974) Algorithm	Pasquill-Turner (1964); Drop One Stability Class	Pasquill-Turner (1964) Approach	Number of Cases*
$\dfrac{\sigma_y \text{ meas**}}{\sigma_y \text{ pred}}$	0.94 ± 0.19	0.89 ± 0.25	0.74 ± 0.19	1.09 ± 0.29	26
$\dfrac{\sigma_z \text{ meas**}}{\sigma_z \text{ pred}}$	0.91 ± 0.18	0.81 ± 0.21	1.27 ± 0.46	3.08 ± 1.05	18
$\dfrac{c_{\text{pred}} \dagger}{c_{\text{meas}}}$	0.98 (1.87)	1.76 (2.09)	0.16 (12.54)		8

* Each case represents an average of repeated measurements. Data used in analysis of the "two-thirds law" and Lamb and Brookhaven-Weil approach approximate 1-hour averages; data used for comparison to the Pasquill-Turner approach approximate 10-minute averages.

** Ratios are arithmetic means + one standard deviation.

† Top ratio is geometric mean; bottom value in parentheses is geometric standard deviation.

agreement with the measurements, being somewhat better for the Pasquill D class curve (see Table 4). However, measured σ_z's are about a factor of 3 higher than the class D predictions and even somewhat higher than the class C curve. The underestimated σ_z's result in overestimates of the distance x_{max} and explain why predicted ground-level concentrations using the PGT approach in the Gaussian model underestimate measured concentrations close to the stacks ($x < x_{max}$), as shown in Table 3 (Pasquill stability class dropped by one). Predicted concentrations using the unmodified PGT approach (no shift in stability class) generally were several orders of magnitude less than measured values and are not shown in Table 3.

The results found here using the empirical dispersion estimates are generally consistent with those found in earlier studies of stack plume dispersion at Maryland power plants (Weil, 1974, 1977). Further discussion of reasons for differences between the measurements and predictions is given by Weil (1978).

Martin Marietta Environmental Center

V. CONCLUSIONS

Lidar measurements of the rise and growth of plumes from the Morgantown power plant stacks were used to assess plume rise and dispersion models.

The following conclusions were drawn:

1. Plume-borne aerosols were found to be good tracers of stack-emitted SO_2. The shape and width of the aerosol profiles obtained by lidar were similar to SO_2 profiles obtained with a Barringer correlation spectrometer in a mobile van.

2. The observed initial plume rise with two stacks operating showed a rise enhancement relative to observed rise with only one stack operating. Observed rise with two stacks operating was close, on the average, to predictions given by the "two-thirds law" using the sum of the buoyancy fluxes from the two stacks. Initial observed rise with one stack operating agreed well with predictions of the "two-thirds law."

3. The instantaneous crosswind and vertical dispersions and the time-averaged, vertical dispersion during initial rise of the buoyant plume were linearly proportional to rise as given by the "two-thirds law", but the proportionality constants were different for the single and two-stack plume observations. A significant feature of these measurements is that they extended almost 5 km downwind of the stacks.

4. Briggs' (1975) formulas for turbulence-limited final rise in neutral or convective conditions agreed well with measurements of turbulence-limited final rise and with all measured maximum plume rises. The lowest predicted final rise from three formulas, one for neutral conditions (equation 9), and two for convective situations (equations 10 and 11), was chosen as the best estimate of final rise; the conclusion given here is based on the comparison between the lowest predicted rise and the observed rise in each case.

5. Briggs' (1970) model for final rise in neutral conditions consistently underestimated measurements of turbulence-limited final rise and all measure' maximum plume rises. The lower of the rise predictions from Briggs' original formulation (equations 3 and 4) and Weil's (1974) modification to it (equations 3 and 7) was chosen as the best estimate of a final rise. Briggs' original formulation gave a lower estimate of final rise in all cases.

6. A combination of the dispersion predictions from the "two-thirds law" and Lamb's (1978b) results for diffusion of neutrally buoyant particles in convective mixing layers yielded dispersion estimates that agreed well with observations. Ground-level SO_2 concentrations predicted using the Gaussian model and the above procedure for computing σ 'd σ_z were equal, on the average, to observed SO_2 concentrations; the geometric standard deviation of the ratio of predicted-to measured

concentration was 1.9. Dispersion predictions using the "two-thirds law" and Lamb's results also agreed better with observations than estimates given by the Brookhaven-Weil (1974) or the Pasquill, Gifford, Turner (1964) methods.

VI. REFERENCES

Briggs, G.A. 1969. Plume Rise. U.S. Atomic Energy Commission, TID-25075, 81 pp.

Briggs, G.A. 1970. Some recent analyses of plume rise observations. Paper presented at 2nd International Clean Air Congress. Washington, D.C., Paper No. ME-8E.

Briggs, G.A. 1974. Plume rise from multiple sources. Air Resources, Atmospheric Turbulence and Diffusion Laboratory, National Oceanographic and Atmospheric Administration. Oak Ridge, Tennessee, ATDL No. 91.

Briggs, G.A. 1975. Plume rise predictions. In Lectures on Air Pollution and Environmental Impact Analyses, American Meteorological Society, Boston, Mass., pp. 59-111.

Browell, E.V. 1977. Lidar remote sensing of tropospheric pollutants and trace gases - programs of NASA Langley Research Center. In proceedings of Fourth Joint Conference on Sensing of Environmental Pollutants, New Orleans, La., November 6-11, 1977.

Csanady, G.T. 1973. Turbulent Diffusion in the Environment. D. Reidel Publishing Co., Boston, Mass. 248 pp.

Deardorff, J.W. 1972. Numerical investigation of neutral and unstable planetary boundary layers. J. Atmos. Sci. 29:91-115.

Deardorff, J.W. 1974. Three-dimensional study of the height and mean structure of a heated planetary boundary layer. Boundary Layer Met. 7:81-106.

Engineering Test Services. 1977. Source testing for the lidar evaluation at the PEPCO Morgantown generating station, Morgantown, Maryland, September - October 1976. Report by Engineering Test Services, Sandston, Va.

Hamilton, P.M. 1967. "Paper III: Plume height measurements at Northfleet and Tilbury power stations." Atmos. Environ. 1:379-387.

Johnson, W.B. and Uthe, E.E. 1971. Lidar study of the Keystone stack plume. Atmos. Environ. 5:703-724.

Lamb, R.G. 1978a. A numerical simulation of dispersion from an elevated point source in the convective planetary boundary layer. Atmos. Environ. 12:1297-1304.

Lamb, R.G. 1978b. The effects of release height on material dispersion in the convective planetary boundary layer, Draft, Division of Meteorology, U.S. Environmental Protection Agency, Research Triangle Park, N.C.

Mills, R.S., Allen, R.J., and Butler, C.F. 1978. An experimental/analytical program to assess the utility of lidar for pollution monitoring, Prepared by Department of Physics and Geophysical Sciences, Old Dominion University, Norfolk, Va., Technical Rept. PG STR-AP 78-9.

Taylor, G.I. 1921. Diffusion by continuous movements. Proc. London Math. Soc. 20:196-212.

Turner, D.B. 1964. A diffusion model for an urban area. J. Appl. Meteor. 3:83-91.

Weil, J.C. 1974. Comparison between measured and model-estimated ground-level SO$_2$ concentrations downwind from the Dickerson Power Plant, prepared by Martin Marietta Laboratories for Maryland Power Plant Siting Program, Department of Natural Resources, Ref. No. PPSP-MP-11.

Weil, J.C. 1977. Evaluation of the Gaussian plume model at Maryland power plants, prepared by Martin Marietta Environmental Technology Center for Maryland Power Plant Siting Program, Department of Natural Resources, Ref. No. PPSP-MP-16.

Weil, J.C. 1978. Applicability of stability classification schemes and associated parameters to dispersion of tall stack plumes in Maryland. Submitted to Atmos. Environ.

Weil, J.C. and Jepsen, A.F. 1977. Evaluation of the Gaussian plume model at the Dickerson Power Plant. Atmos. Environ. 11:901-910.

Willis, G.E. and Deardorff, J.W. 1974. A laboratory model of the unstable planetary boundary layer. J. Atmos. Sci. 31: 1297-1307.

Willis, G.E. and Deardorff, J.W. 1978. A laboratory study of dispersion from an elevated source within a modeled convective planetary boundary layer. Atmos. Environ. 12:1305-1312.

APPENDIX A

Data Used In Analysis

Nomenclature for Tables A1 - A6

A. Lidar Backscatter and SO_2 Profile Results (Tables A1 and A4)

RUN = an identification code for each set of lidar (or SO_2) profiles and associated meteorological and power plant conditions

START TIME = time at which repeated lidar scans or mobile van traverses began for a particular cross section; first two digits are the hour, last two digits are minutes after the hour

END TIME = time at which repeated scans or van traverses ended for a cross section

x = radial distance from power plant to the centroid of the average scattering ratio (SR) lidar distribution or the average crosswind SO_2 profile; average profile computed from N repeated scans or traverses (m)

z = height of centroid of average lidar SR distribution at the stack (m)

σ_y = crosswind standard deviation computed from average lidar SR distribution or average crosswind SO_2 profile (m)

σ_z = vertical standard deviation computed from average lidar SR distribution (m)

$\langle\sigma_y\rangle$ = average of N individual crosswind standard deviations from repeated lidar scans or repeated SO_2 profiles at a cross section (m)

$\langle\sigma_z\rangle$ = average of N individual vertical standard deviations from repeated lidar scans at a cross section (m)

N = number of lidar scans or SO_2 profiles in a set of repeated measurements at a cross section

PHI = angular bearing of centroid of average crosswind SO_2 profile; angle measured clockwise from grid north (deg)

c_2 = maximum SO_2 ground-level concentration from average crosswind SO_2 profile (ppb)

std_2 = standard deviation in SO_2 concentration about c_2 (ppb)

c_1 = average of individual maximum SO_2 ground-level concentrations from N repeated crosswind profiles at a cross section (ppb)

std_1 = standard deviation in SO_2 concentration about c_1 (ppb)

Martin Marietta Environmental Center

B. Power Plant Operating Conditions (Tables A2 and A5)

Q_1, Q_2 = SO_2 emission rate for stack 1 and stack 2, respectively, computed from fuel consumption and fuel analysis (composition) data (kg/sec)

F_1, F_2 = buoyancy flux from stack 1 and 2, respectively, Briggs (1970) definition of buoyancy flux (m^4/sec^3).

C. Meteorological Conditions (Tables A3 and A6)

v = average wind speed in mixing layer (m/sec)

THETA = average wind direction in mixing layer; direction from which wind blows; direction measured clockwise from grid north (deg)

T_1 = average ambient temperature at surface (°C)

DTDZ = average potential temperature gradient between stack top and top of mixing layer (°C/m)

H_m = depth of mixing layer (m)

Q_R = solar insolation ($cal/cm^2/hr$)

HR = hour at which surface meteorological observations were obtained from airport weather data

CLC = cloud cover in tenths from airport weather data

CEL - ceiling height; unlimited ceiling height given by 999 (hundreds of feet)

VS = surface wind speed at airport (m/sec)

Table A1. Lidar measurements.

| Date | | | Run | Start Time | End Time | x | Eulerian Averages | | | Arithmetic Mean | | N |
Day	Mon.	Year					z	σ_y	σ_z	$\langle\sigma_y\rangle$	$\langle\sigma_z\rangle$	
22	9	76	2L	1558	1619	3210	192	241	222	227	153	10
22	9	76	3L	1638	1744	2152	608	242	286	155	204	6
				1630	1748	3162	792	236	291	230	246	8
				1648	1751	4888	736	354	448	313	386	6
23	9	76	5L	1337	1410	2287	294	252	167	232	117	8
				1338	1411	3471	325	251	189	225	172	7
				1340	1412	4564	485	314	201	262	186	8
23	9	76	6L	1529	1604	1004	262	143	104	98	62	7
				1531	1607	2137	352	236	226	104	129	7
				1530	1608	2979	502	274	229	167	166	14
24	9	76	8L	1253	1335	1524	540	211	175	168	171	5
				1255	1337	2527	657	343	187	315	176	5
15	10	76	9L	1142	1158	1142	140	84	88	69	75	14
15	10	76	10L	1217	1236	2114	286	192	130	184	103	9
15	10	76	11L	1354	1454	415	71	60	46	76	34	8
				1356	1455	1544	170	115	117	132	105	9
				1358	1501	2506	225	213	177	192	150	19

Martin Marietta Environmental Center

Table A1. (cont'd.)

Date			Run	Start Time	End Time	x	Eulerian Averages			Arithmetic Mean		N
Day	Mon.	Year					z	σ_y	σ_z	$<\sigma_y>$	$<\sigma_z>$	
26	10	76	12L	1700	1801	841	124	210	85	291	70	11
				1702	1806	2036	179	243	115	212	90	10
				1704	1808	3207	254	279	140	235	139	10
				1705	1810	4422	246	367	160	300	170	9
27	10	76	13L	1433	1547	1429	353	271	192	265	151	4
				1435	1550	2421	535	362	275	232	223	4
				1440	1610	3941	636	510	360	386	338	6
				1443	1614	5121	527	260	308	220	306	3
28	10	76	14L	1025	1113	1342	169	254	139	245	130	6
				1027	1135	2211	293	317	212	324	222	7
				1030	1138	3659	456	334	261	343	269	7
				1034	1147	4951	553	568	300	514	324	7
				1036	1154	6074	528	383	365	428	373	7
28	10	76	15L	1516	1632	2682	456	276	282	207	229	10

Table A2. Meteorological conditions for lidar data

Day	Month	Year	Run	v	THETA	T_1	DTDZ	H_m	Q_R	IR	CLC	CEL	VS
22	9	76	2L	13.7	306	18	0.0	1650	48.0	16	0	999	6.2
22	9	76	3L	6.7	298	18	0.0	1650	30.0	16	0	999	6.2
23	9	76	5L	8.4	22?	24	0.0	1200	61.8	13	5	999	7.7
23	9	76	6L	7.3	211	21	0.0	1200	43.2	16	8	999	8.8
24	9	76	8L	4.3	50	19	0.0018	1100	42.9	13	8	999	3.6
15	10	76	9L	10.8	228	19	0.0	700	63.6	13	0	999	9.3
15	10	76	10L	10.0	224	19	0.0	700	64.2	13	0	999	9.3
15	10	76	11L	12.1	234	23	0.0008	1200	56.4	16	0	999	7.2
26	10	76	12L	11.9	358	7	0.008	1250	7.2	19	0	999	9.3
27	10	76	13L	5.8	1	3	0.0013	1250	27.1	16	10	100	7.?
28	10	76	14L	6.2	12	5	0.0003	1100	46.2	10	6	999	?.1
28	10	76	15L	5.5	313	5	0.0008	1200	33.0	16	2	999	4.1

Martin Marietta Environmental Center

Table A3. Plant conditions for lidar data

Day	Month	Year	Run	Q_1	F_1	Q_2	F_2
22	9	76	2L	1.73	737	1.70	724
22	9	76	3L	1.73	741	1.73	741
23	9	76	5L	1.74	704	1.63	704
23	9	76	6L	1.75	723	1.65	723
24	9	76	8L	1.69	724	1.76	736
15	10	76	9L			1.65	741
15	10	76	10L			1.64	742
15	10	76	11L			1.61	717
26	10	76	12L			1.79	819
27	10	76	13L			2.02	...
28	10	76	14L			2.04	831
28	10	76	15L			2.06	825

Table A4. Mobile van measurements.

| Date | | | Run | Start Time | End Time | x | PHI | Ground-level SO$_2$ Profiles | | | | | | | Vertically Integrated SO$_2$ Profiles | |
| | | | | | | | | Average Profile | | | Arithmetic Means | | | | Average Profile σ_y | Arithmetic Mean $\langle\sigma_y\rangle$ |
Day	Month	Year						c_2	std_2	σ_y	c_1	std_1	$\langle\sigma_y\rangle$	N		
22	9	76	1MV	1047	1215	2401	130	9	17	495	18	19	468	8	214	140
			2MV	1359	1522	8918	117	37	36	670	50	31	464	6	688	602
			3MV	1645	1736	3441	110	15	15	525	32	17	281	4	389	290
23	9	76	4MV	1320	1414	5694	28	76	90	426	90	81	417	4	595	532
			5MV	1524	1609	2734	32	10	14	262	18	18	134	6	196	159
24	9	76	6MV	1154	1306	12271	207	45	32	2484	63	38	1284	5	1112	966
27	10	76	7MV	1509	1554	25523	162	15	1	2138	16	1	1922	3	NA*	NA
28	10	76	8MV	1607	1642	2221	116	16	26	775	30	29	318	6	388	320

*NA profiles were not measured because integrated SO$_2$ levels were below the sensitivity of the correlation spectrometer.

A-7

Martin Marietta Environmental Center

Table A5. Meteorological conditions for mobile van data

Day	Month	Year	Run	v	THETA	r_1	DTDZ	H_m	Q_R	HR	CLC	CEL	VS
22	9	76	1MV	9.4	309	17	0.0	1650	69.0	10	1	999	7.2
			2MV	7.6	299	20	0.0	1650	68.4	16	0	999	6.2
			3MV	6.7	298	20	0.0	1650	35.0	16	0	999	6.2
23	9	76	4MV	8.4	224	24	-0.0012	1200	63.8	13	5	999	7.7
			5MV	7.2	211	21	+0.0020	1200	46.8	16	8	999	8.8
24	9	75	6MV	4.6	59	20	-0.0020	1100	49.8	13	8	999	3.6
27	10	75	7MV	5.8	1	3	0.0010	1250	22.2	16	10	760	7.2
28	10	76	8MV	5.5	313	5	0.0	1200	33.0	16	2	999	4.1

Table A6. Plant conditions for mobile van data

Day	Month	Year	Run	Q_1	F_1	Q_2	F_2
22	9	76	1MV	1.72	750	1.67	754
			2MV	1.73	723	1.49	601
			3MV	1.73	727	1.73	728
23	9	76	4MV	1.74	705	1.66	705
			5MV	1.74	721	1.65	723
24	9	76	6MV	1.72	722	1.78	730
27	10	76	7MV			1.64	718
28	10	76	8MV			1.61	718

APPENDIX B

Comparison Between Crosswind Profiles of Scattering Ratio and SO_2

by

Jonathan L. Altman

One of the objectives of this study was to evaluate the usefulness of the lidar for inferring SO_2 distributions in buoyant stack plumes. The first step in such an evaluation is to compare data obtained with the lidar to similar data obtained by some other method. We have chosen to use the vertically integrated SO_2 distribution in the plume measured by a Barringer correlation spectrometer (COSPEC) for the comparison. We have routinely used that instrument in the past to obtain information about the SO_2 distribution of the elevated plume. The lidar backscatter data can be processed to give the vertically integrated scattering ratio in sections through the plume. As discussed in the footnote on page II-3, the scattering ratio is a measure of the relative particulate mass concentrations in the plume.

In making the comparison between these two sets of data, two basic assumptions were made. First, we assumed that the settling velocities of the particles in the plume were small enough that the particulates were dispersed in the same way as a gas. Second, we assumed that the proportion of suspended particulates to SO_2 gas in the stack effluent was constant during the time required for one set of lidar and COSPEC measurements. Both these assumptions require close scrutiny in the light of the results of the comparison.

The lidar and COSPEC measurements were compared for five sets of simultaneously taken data. Dates and configurations under which these data sets were taken are given in the first four columns of Table B1 and in the maps of Figures B1 to B4. Since a single crosswind profile takes longer to obtain

B-1

with the COSPEC than with the lidar, because of the van's travel time, we have made no attempt to directly compare individual crosswind profiles; instead, an averaged profile for the time periods indicated was calculated. The results were then compared on the basis of (1) the shapes and widths of the profiles (qualitative comparison), (2) the crosswind standard deviations (σ_y) (quantitative comparison), and (3) locations of the centroid of the vertically integrated concentration distributions.

The lidar data were initially analyzed to give the vertically integrated scattering ratio as a function of distance along the lidar line of sight for each lidar scan. The distance along this line was then divided into 200-meter segments, and the integrated scattering ratios falling within each segment were summed. The sums for a given segment from each of the individual profiles within a given time period were then averaged, and each of the averages was divided by the maximum average value obtained for all the segments. Thus, an average profile normalized to unity at its peak was obtained for the appropriate time interval. Since the scattering ratio is proportional to the concentration of aerosols, the normalized profile just described is effectively a normalized concentration profile of aerosols. This profile was com, ed with a similarly normalized averaged COSPEC concentration profile of SO_2 ov the same run. The standard deviations of each of the segmental averages were also computed and were normalized by the average scattering ratio for the appropriate segment.

The vertically integrated SO_2 concentration, or SO_2 burden, obtained by the COSPEC was analyzed similarly to the lidar data. For each individual SO_2 profile, the SO_2 burden was summed within the same crosswind segments used for computing the scattering ratio "sums". Fig. Bl illustrates this geometry. Normalized averages and st dard deviations of the SO_2 burden "sums" were then computed for each crosswind segment by the same method used for the computation

of the lidar profiles. Plots of these normalized average "sums" and their standard deviations for both the lidar and COSPEC measurements are shown in Figs. B5 through B9.

A visual comparison of the profiles in Figs. B5 through B9 reveals fair overall agreement. The most obvious differences between the lidar and COSPEC profiles seem to be their relative displacement rather than any great differences in shape (with the exception of Fig. B8). The best agreement was obtained for the two profiles on 22 September.

Table B1 summarizes several parameters which give a quantitative measure of the crosswind dispersion, as well as the variability of the plume position during the measurement time. We found that, in every case, σ_y of the individual COSPEC profiles was greater than that for the lidar profile. This was also true in all but one case (25 Sept.; 1524-1609) for the σ_y of the averaged profile. The difference may be related to the difference in sampling time for the two instruments. The typical time required for a lidar scan is 1 minute, while the van carrying the COSPEC requires 3 to 5 minutes to complete a single pass under the plume.

The variation of the plume position is expressed in columns seven and eight of Table B1 as the standard deviation in both degrees and meters of the crosswind position of the centroids of the individual profiles. These values were calculated by taking the second moment of the angular position of the individual centroids about the mean centroid position. The lidar and COSPEC data show a marked disagreement in calculations of this parameter; however, the difference is not consistent as it was for the σ_y computations. It should be noted, however, that the two sets of data taken by the same method on the same day are consistent. Thus, both sets of COSPEC measurements on 23 September show a less variable plume than do the lidar, while the reverse

Martin Marietta Environmental Center

is true on 22 September. A closer examination of individual lidar profiles on the afternoon of 23 September revealed a fairly large variation in the scattering ratio profiles both horizontally and vertically. In addition, the wind profiles from that time period showed relatively large wind direction shear ($\sim 0.035°/m$).

Although our data were not sufficiently detailed to indicate with any certainty the reasons for the differences between the lidar and the COSPEC measurements, there are several likely causes. We feel that the most important reason for the discrepancies is the difference in cross-section sampling time for the lidar and the COSPEC. In most cases, COSPEC profiles would be expected to be somewhat wider than the lidar profiles because of the wandering of the plume during the longer measurement time. This wandering would also affect the measures of plume variation (σ_y and plume centroid location) and depends on the time scale of the largest atmospheric eddies. Thus, the effects of time differences during cross-section sampling vary with the meteorological conditions (ambient turbulence time scale). Another factor which may have caused a difference between the lidar and COSPEC measurements is the possibility that the proportion of aerosol to SO_2 in the plumes was not always constant. Based on visual observations and the stack test data, we suspect that the stack particulate flux over short time intervals (several minutes) varied much more than the stack SO_2 flux. Constant stack fluxes of SO_2 and particulates during the measurements would be highly desirable in any future work.

Table B1. Computed plume parameters from lidar and COSPEC data

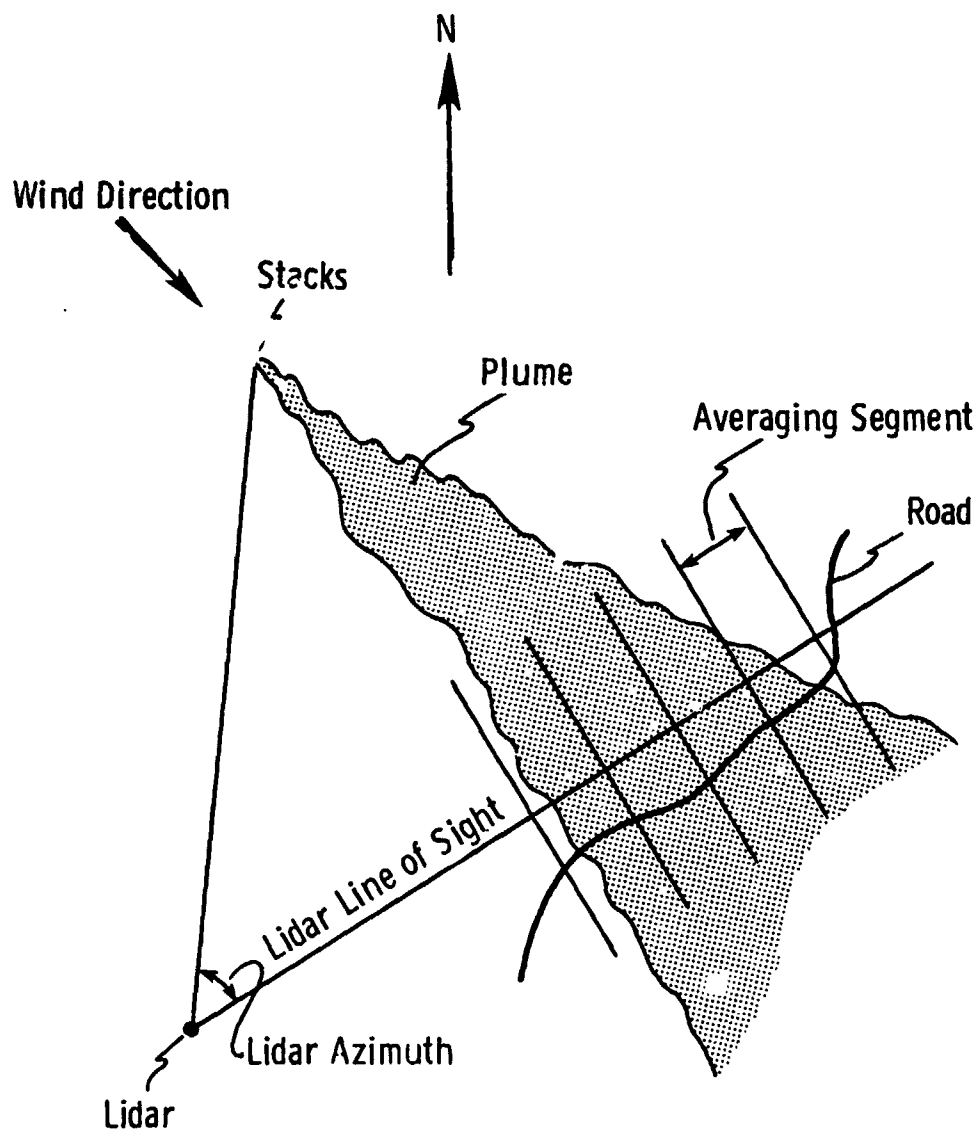|	Date	Time	No. of Indiv. Profiles	Centroid Distance From Stacks (m)	σ_y of Avg Profile (m)	Avg of σ_y Indiv. Profile (m)	Std. Dev. of Centroid Crosswind Pos. (m)	Std. Dev. of Centroid Crosswind Pos. (Deg)	Centroid Angular Pos. (Deg. from North)
COSPEC	9/22	1557-1638	4	3441	387	260	259	4.32	108
Lidar	9/22	1558-1619	10	3210	241	227	149	2.66	109
COSPEC	9/22	1645-1736	5	3441	389	291	209	3.48	109
Lidar	9/22	1629-1748	8	3162	251	230	152	2.75	112
COSPEC	9/23	1119-1215	4	2833	250	235	75	1.51	28
Lidar	9/23	1131-1214	16	2958	191	173	170	3.27	30
COSPEC	9/23	1524-1609	6	2734	196	159	74	1.56	32
Lidar	9/23	1530-1609	14	2979	209	128	283	5.44	50
COSPEC	10/28	1607-1642	7	2221	388	320	140	3.61	124
Lidar	10/28	1606-1632	4	3010	215	168	130	2.48	120

Martin Marietta Environmental Center

Figure B-1. Plan view of plume and measurement geometry.

Sept. 22, 1976

Mobile Van 1557 - 1638 ; 1645 - 1736
Lidar 1558 - 1619 ; 1629 - 1748

Mobile Van Measurement Route

Lidar Line of Sight

1 km

Lidar

Stacks

N
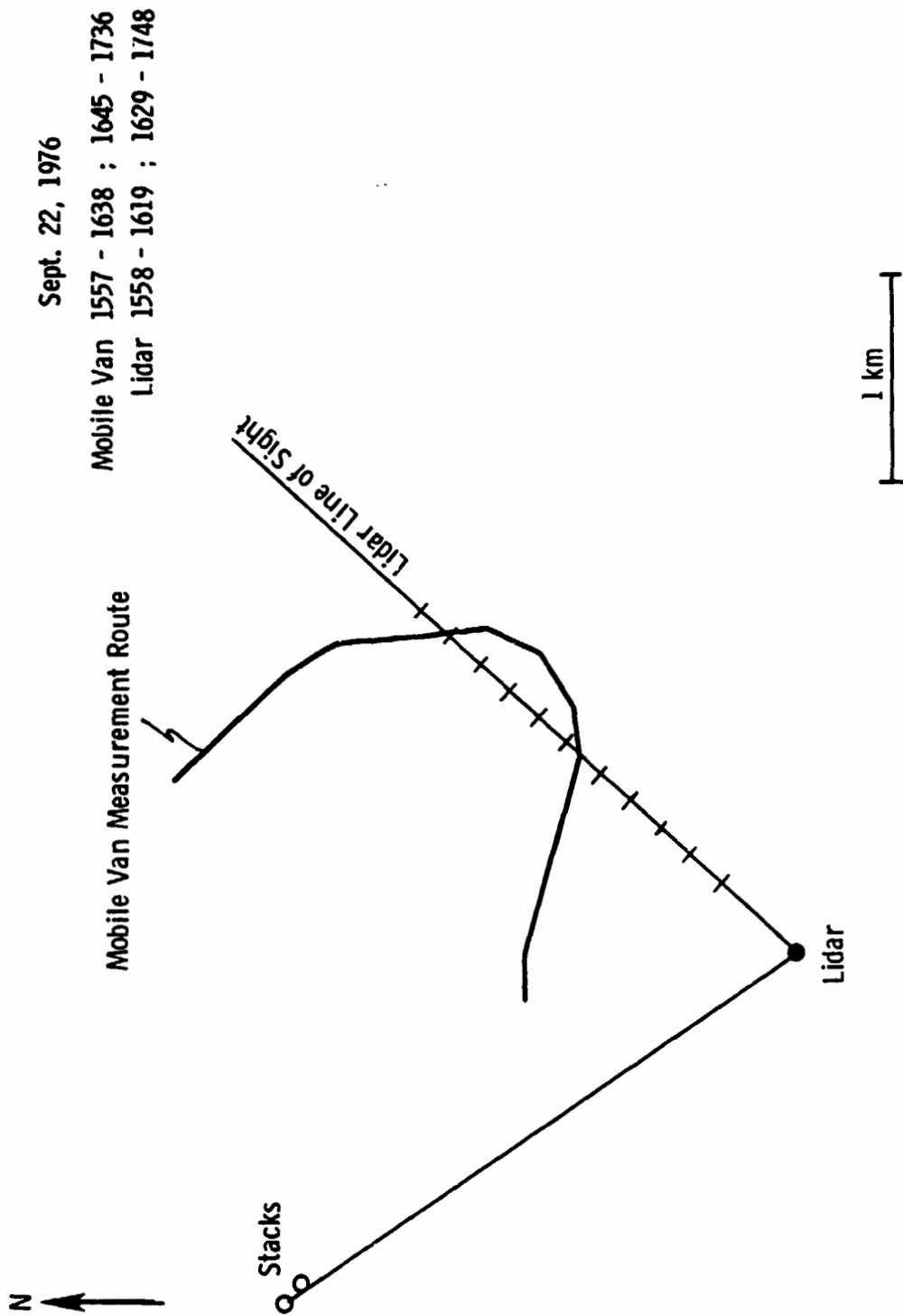
Figure B-2. Measurement route and lidar scan geometry for September 22, 1976.

Martin Marietta Environmental Center
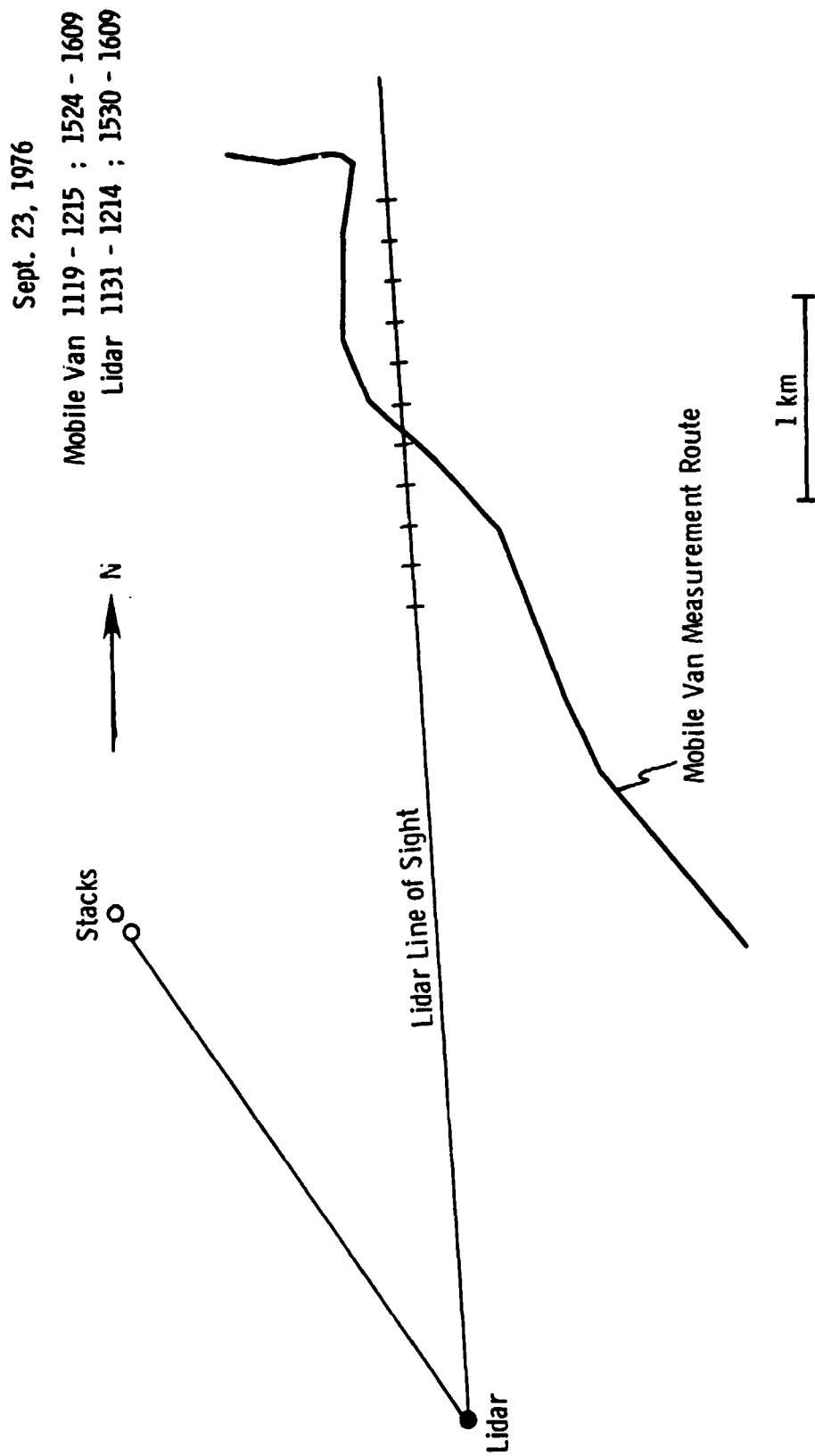
Figure B-3. Measurement route and lidar scan geometry for September 23, 1976.

Sept. 23, 1976

Mobile Van 1119 - 1215 ; 1524 - 1609
Lidar 1131 - 1214 ; 1530 - 1609

N

Stacks

Lidar Line of Sight

Lidar

Mobile Van Measurement Route

1 km

Oct. 28, 1976

Mobile Van 1607 - 1642
Lidar 1606 - 1632

Mobile Van Measurement Route

N

Stacks

Lidar Line of Sight

Lidar

1 km
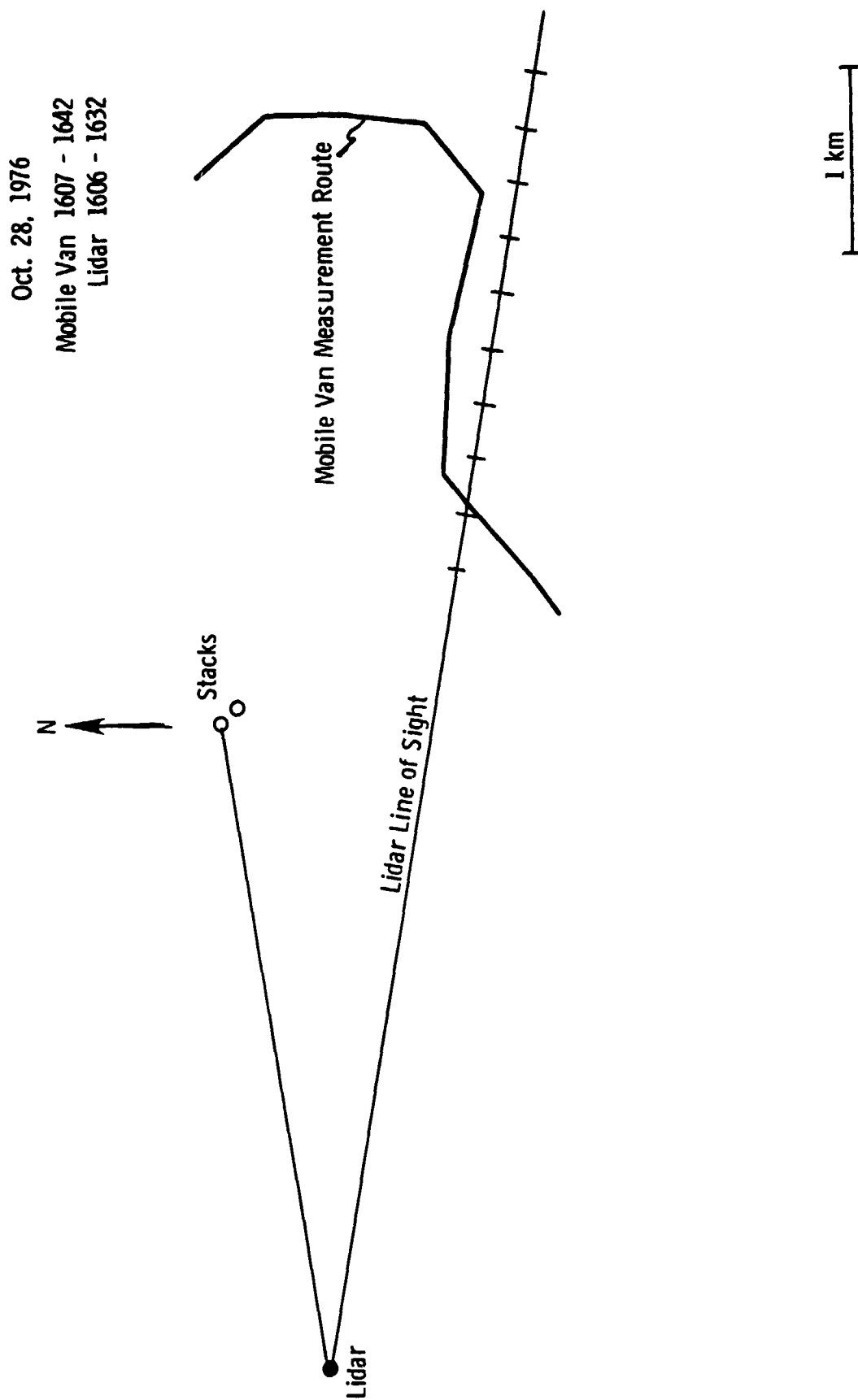
Figure B-4. Measurement route and lidar scan geometry for October 28, 1976.
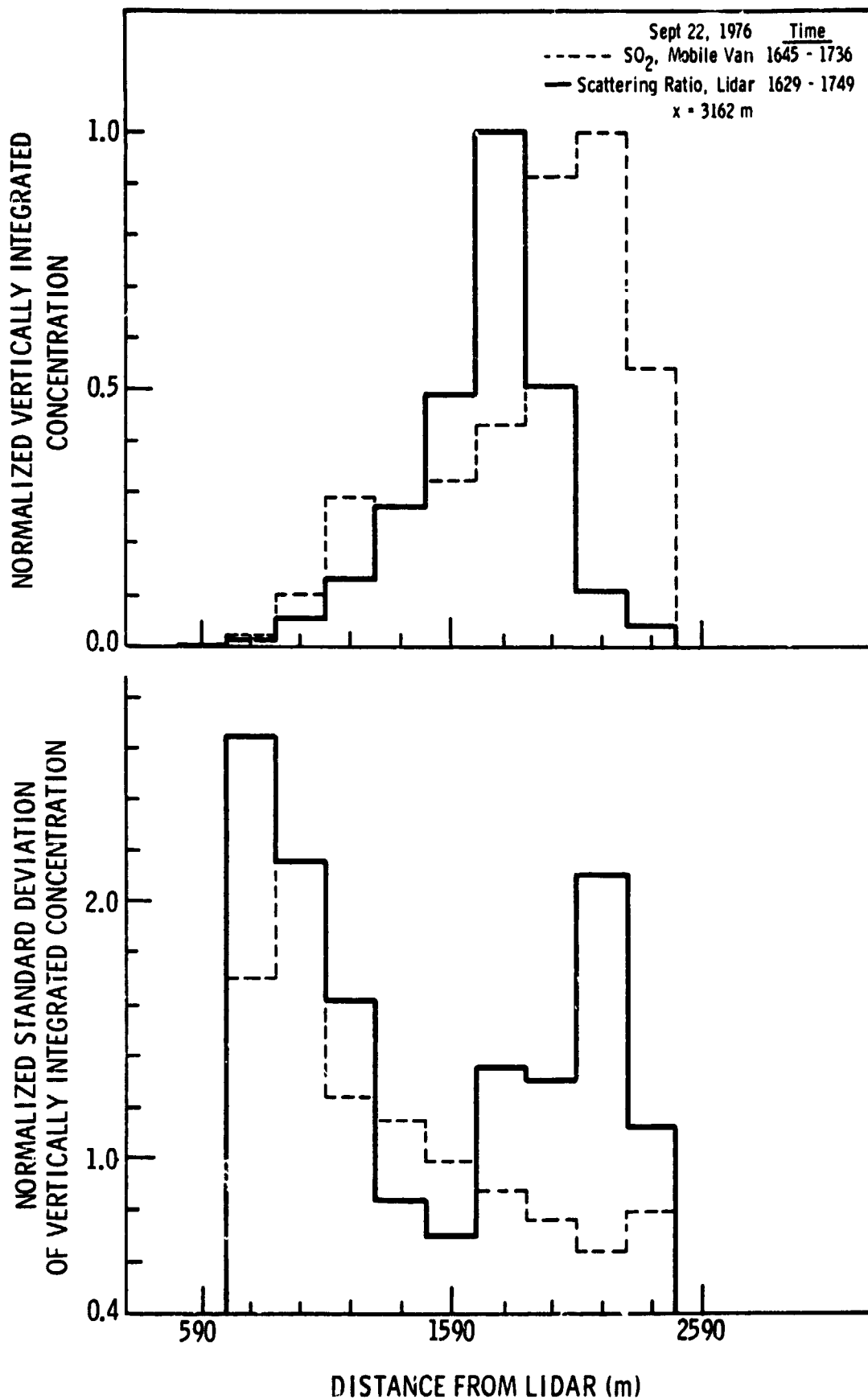
Martin Marietta Environmental Center
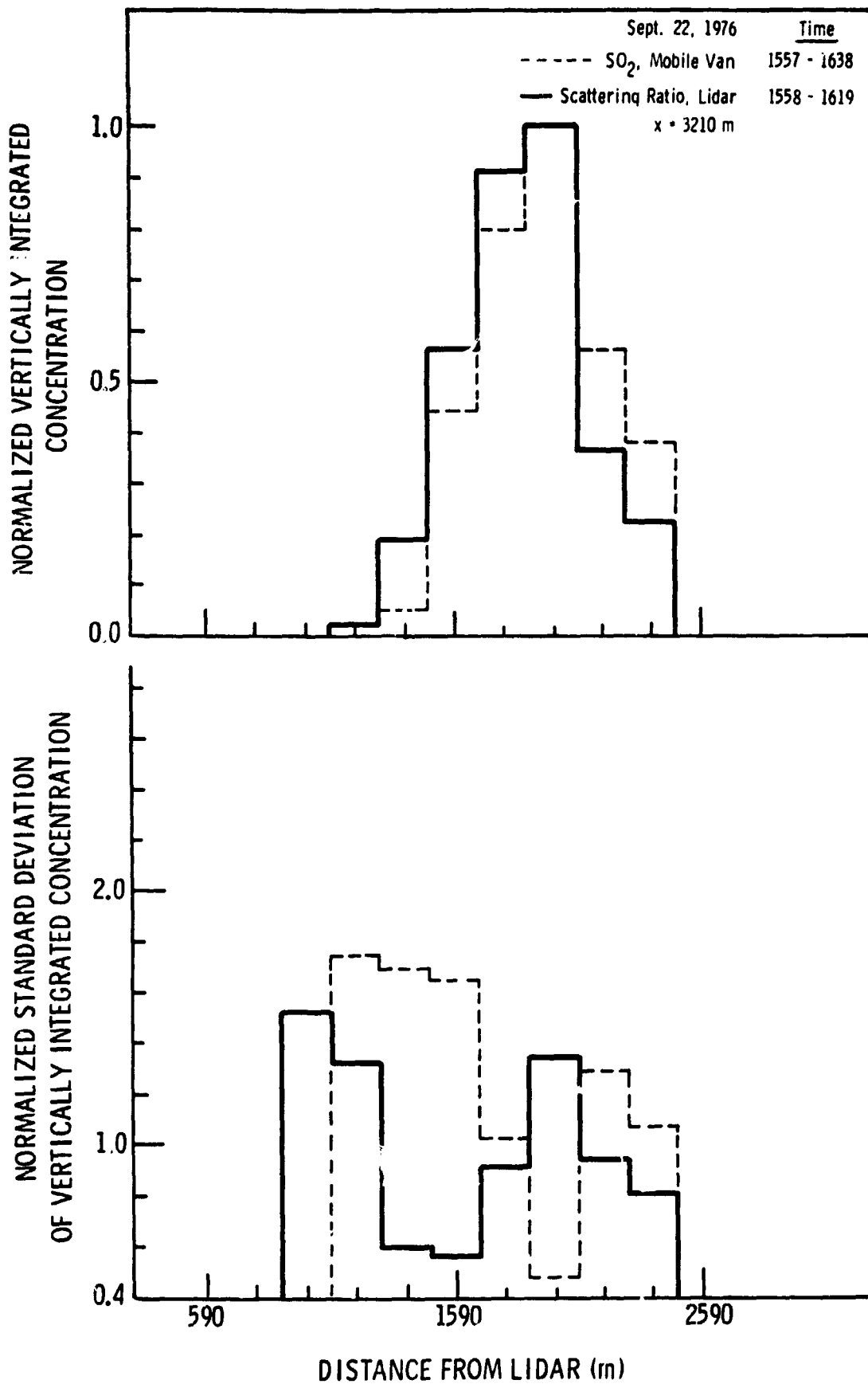
Figure B-5. Normalized average concentrations and standard deviations by crosswind segment.

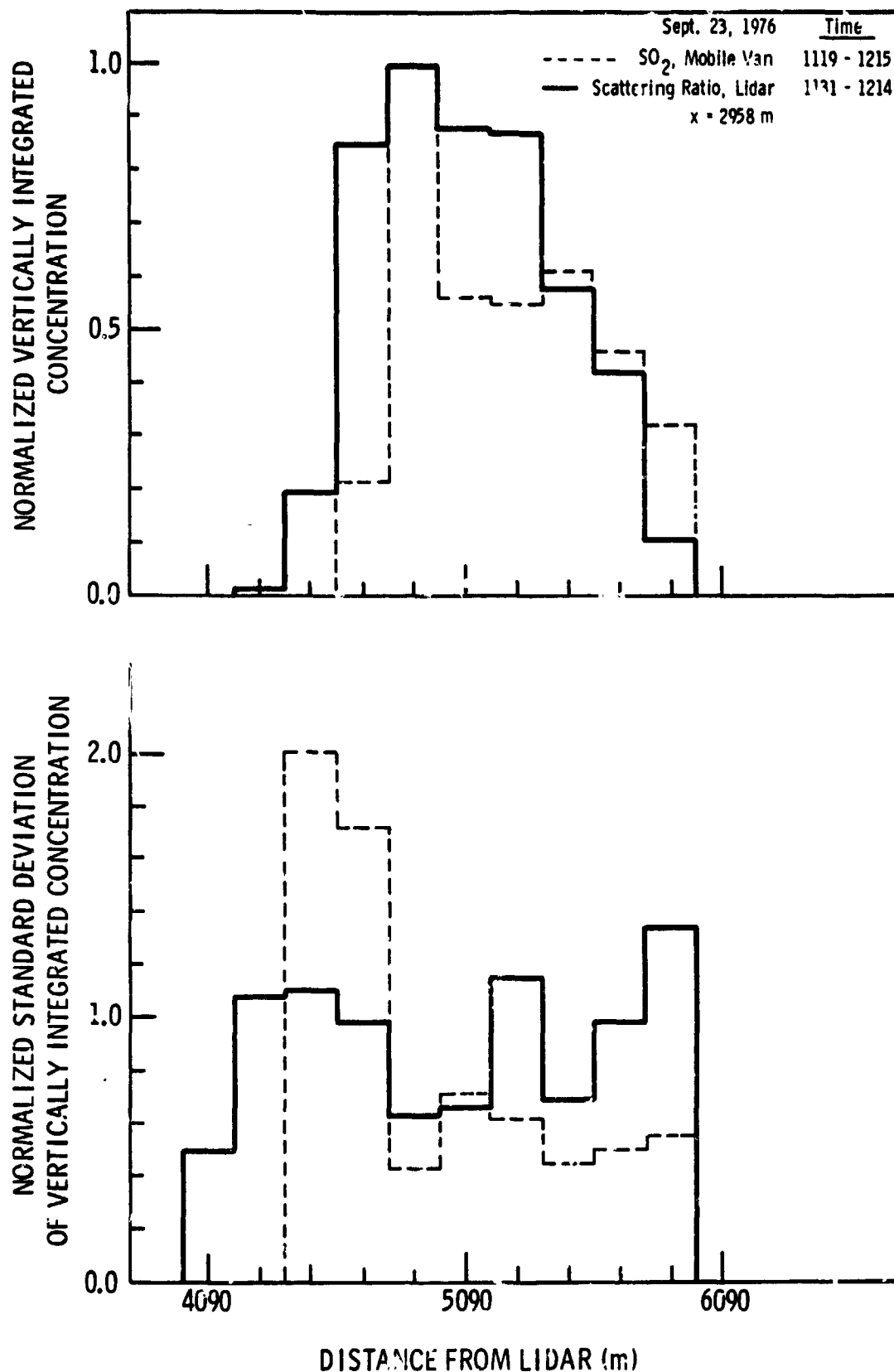Figure B-6. Normalized average concentrations and standard deviations by crosswind segment.
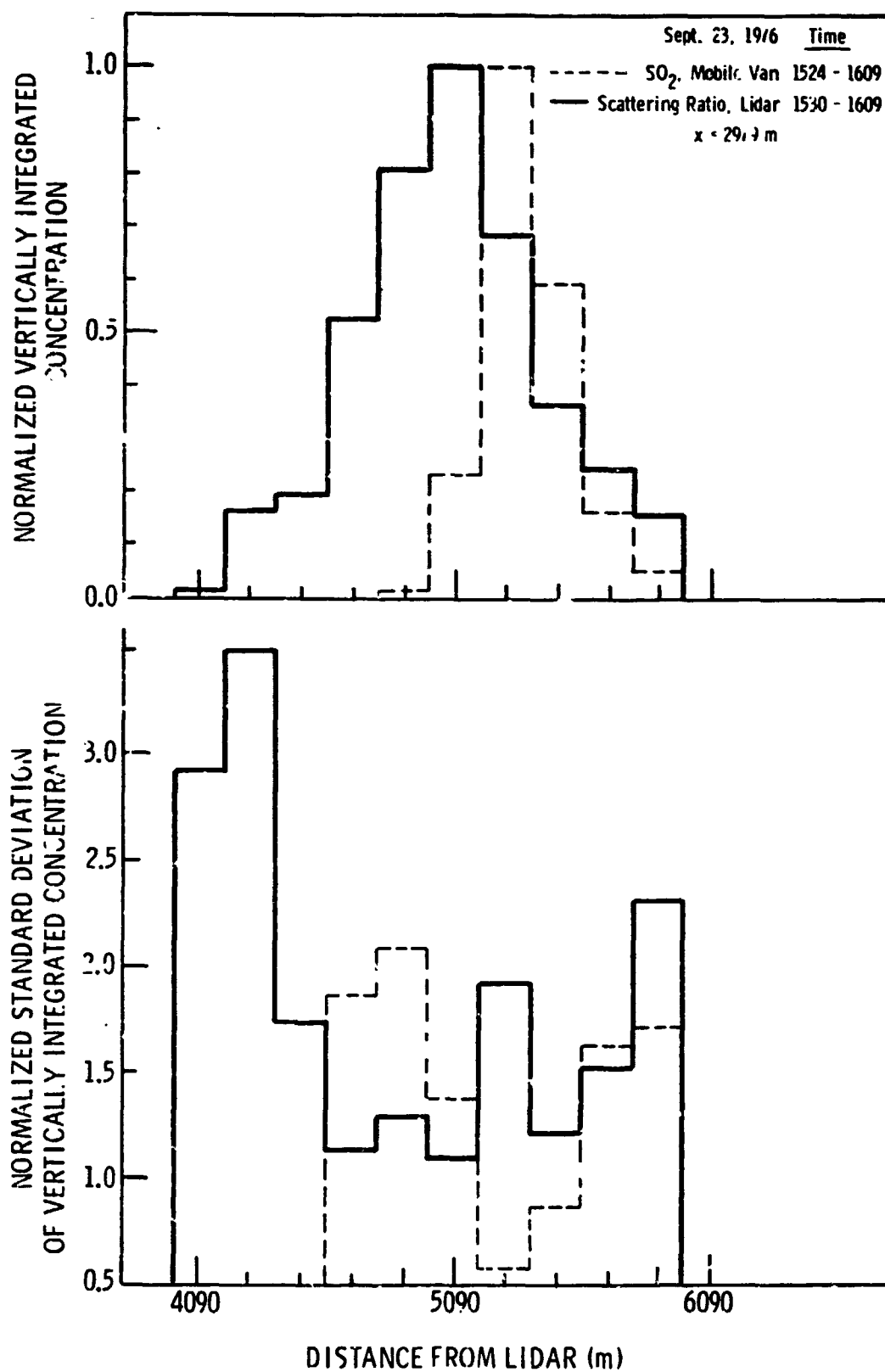
Martin Marietta Environmental Center

Figure B-7. Normalized average concentrations and standard deviations by crosswind segment.

Figure B-8. Normalized average concentrations and standard deviations b; crosswind segment.
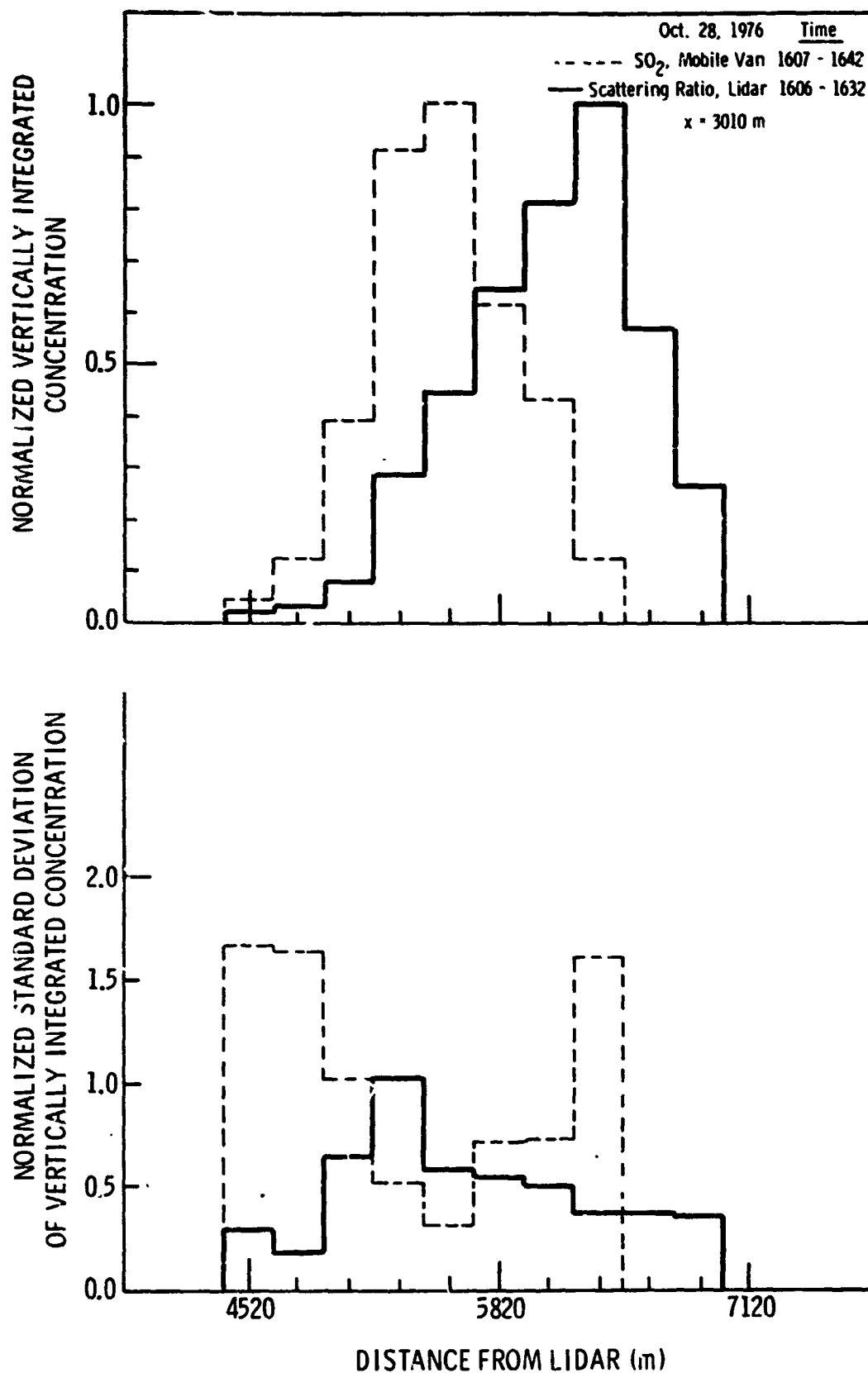
Figure B-9. Normalized average concentrations and standard deviations by crosswind segment.